Toxic effects of combined exposure of Triclosan and Glyphosate on the Zebrafish embryos

A Dissertation Submitted to

Indian Institute of Technology Hyderabad

In Partial Fulfillment of the Requirements for

The Degree of Master of Technology

By

Poonam

(BO18MTECH11008)

Under the guidance of

Dr Anamika Bhargava

भारतीय प्रौद्योगिकी संस्थान हैदराबाद

Indian Institute of Technology Hyderabad

Department of Biotechnology

June, 2020

Declaration

I, Poonam, hereby want to declare that this project report entitled as "**Toxic effects of combined exposure of Triclosan and Glyphosate on the Zebrafish embryos**" presents a record of my original work and ideas in my own language. Also, I have clearly mentioned and cited the original resources' references wherever applicable. I also declare that I have followed all the principles related to academic integrity and morality and have not either forged or fabricated any fact/data/information. I fully understand that any violation of the above will lead to disciplinary action from institution and might also lead to penal action if not appropriately cited or necessary permission has not been granted wherever required

_____

(Signature)

_____

Poonam

_____

BO18MTECH11008

Approval Sheet

This thesis entitled as "**Toxic effects of combined exposure of Triclosan and Glyphosate on the Zebrafish embryos**" by Poonam is accepted for completion of the degree of Master of Technology.

Dr Rajakumara Eerappa
Associate professor
Examiner

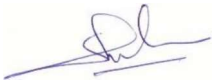

Dr D S Sharada
Associate professor
Examiner

Dr Anamika Bhargava,
Associate professor
Adviser

Dr Basant K Patel
Associate professor
Chairman

Acknowledgements

It fills me up with enormous happiness to thank all people who have graciously helped me throughout this project. Inspirations, consistent encouragement and supervision of these people has facilitated the completion of this project.

Firstly, I want to express my solemn thankfulness to my M. Tech thesis guide Dr Anamika Bhargava, Associate Professor, Department of Biotechnology who have always directed me diligently with her great ideas along with continuous reassurance to work towards my dream of becoming a great researcher. I am enormously grateful to her for scientific and logical understanding she has graced me which will benefit in my future.

Secondly, I also feel greatly indebted towards my Ph.D. research fellows Mr Narasimha and Ms Yashashwini. And last but not the least, my M. Tech classmate as well as lab fellow Mr Chittaranjan Sahu who has always been a great help. All these people blessed me with their extensive personal and professional guidance all through the way till end. Without their support, accomplishment of this project report would have been impossible.

I further want to extend my thanks to Indian Institute of Technology, Hyderabad (IITH) for funding my research work and Ministry of Human Resource Development (MHRD) for their generous fellowship.

Poonam
BO18MTECH11008

Abstract

Triclosan and glyphosate are commonly used chemicals worldwide. While TCS is an antimicrobial compound having application in health care and household; glyphosate is a non-selective herbicide used in agricultural as well as non-agricultural applications. Overuse of both these compounds since past 2-3 decades has raised concerns about its safety on public health. Recently FDA has banned TCS in handwash soaps. But its use in other consumer goods is questionable. On the other hand, glyphosate still remains a source of controversy for its carcinogenic properties. Many studies have analysed toxicity of these chemicals individually. but single exposure is an ideal scenario. Humans are exposed to a variety of different chemicals simultaneously on a daily basis.

We studied the effects of combined exposure of Triclosan and Glyphosate on the Zebrafish embryos. In addition, we investigated the effects of TCS on neuromuscular junction of Zebrafish embryos.

We observed that the combined exposure of TCS and glyphosate is more toxic as compared to individual exposure of TCS or glyphosate. Combined exposure increased mortality rate, delayed hatching, increased morphological abnormalities as well as decreased larval length.

In addition, we observed TCS exposure disrupted the integrity of the NMJ junction in a concentration dependent manner as indicated by an increase in chevron angle and increased visible discontinuities upon labelling of the NMJ by Znp1 antibody which labels motor neuron axons.

Overall, our results indicate that development toxicity is more severe in case of combined exposure in embryos. And also, TCS interferes with integrity of NMJ in zebrafish embryo.

Abbreviations

ADHD	-	Attention deficit hyperactivity disorder
BSA	-	Bovine Serum Albumin
CaP	-	Caudal Primary
CGLS	-	Conjugate Gradient for Least Squares
DMSO	-	Dimethyl Sulphoxide
EFSA	-	European Food Safety Authority
GBHs	-	Glyphosate Based Herbicides
H_2O_2	-	Hydrogen Peroxide
HEK	-	Human Embryonic Kidney
hpf	-	Hours Post fertilization
HyBR	-	Hybrid Bidiagonalization Regularization
IARC	-	International Agency for Research on Cancer
KCl	-	Potassium Chloride
KH_2PO_4	-	Potassium Dihydrogen Phosphate
KOH	-	Potassium Hydroxide
MiP	-	Middle Primary
MRNSD	-	Modified Residual Norm Steepest Descent
NaCl	-	Sodium Chloride
Na_2HPO_4	-	Di-Sodium Hydrogen Phosphate
NHANES	-	National Health and Nutrition Examination Survey
NMJ	-	Neuro-muscular Junction
PBS	-	Phosphate Buffer Saline
PCE	-	Percardial Edema
PID	-	Parallel Iterative Deconvolution
PMNs	-	Primary Motor Neurons
POEA	-	Polyoxyetyleneamine
PSF	-	Point Spread Function
RBL	-	Rat Basophilic Leukaemia
RoP	-	Rostral Primary

SC	-	Spinal Curvature
SMCs	-	Skeletal Muscle Cells
SMNs	-	Secondary Motor Neurons
TB	-	Tail Bending
TCS	-	Triclosan
TND	-	Tail Non-Detachment
RT	-	Room Temperature
WHO	-	World Health Organisation
WPL	-	Wiener Filter Preconditioned Landweber
YSE	-	Yolk Sac Edema

List of Figures

List of tables

Contents

Introduction

1.1 Triclosan

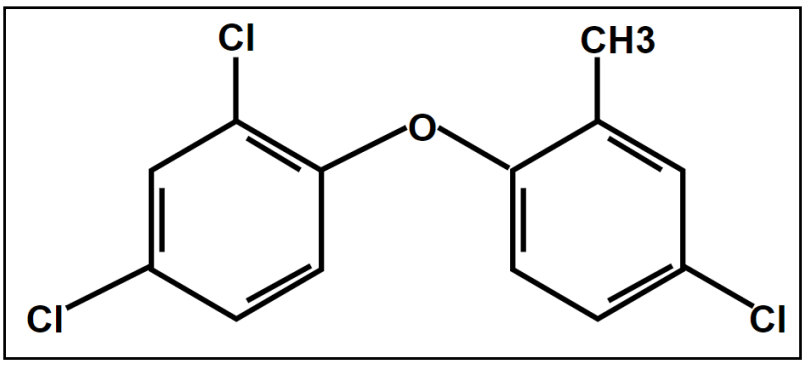

Figure 1. Chemical Structure of Triclosan

Triclosan (also identified as 2,4,4-trichloro-2-hydroxy diphenyl ether; TCS) is a powdered synthetic organic compound with antibacterial and antifungal properties. In 1960s, a Swiss company cida-Geigy developed and patented TCS for the first time (Boyce et al. 2002). It has been extensively used ever since in many health care goods like soaps, liquid sanitizers; personal care product such as deodorants, mouthwash, shaving gels; beauty care products like lip gloss, moisturizers; childrens' toys; kitchenware like cutting boards, semi-automated slicer and other products such as humidifier, vacuum cleaner, interior paints etc. (Weatherly and Gosse 2017)

Table 1. General Properties of TCS

Physical appearance	White-coloured powder
Chemical formulation	$C_{12}H_7Cl_3O_2$
Molecular weight	289.54 g mol-1
Melting point	55-57˚C
Boiling point	120˚C
Density	1.49 g/cm3
Solubility	Acetone

Its ever-increasing use has raised safety concerns about its exposure limit to humans, animals and environment. Earlier reports on triclosan implemented that its antimicrobial properties rely on its ability to inhibit of a specific enzyme involved in the fatty acid

synthesis in microorganisms; hence specific for microorganisms (Chuanchuen et al. 2001; Heath et al. 2000; Hoang and Schweizer 1999; Slayden, Lee, and Barry 2000) . Later on, it was found to be wrong (Liu et al. 2002). TCS has been reported to involved in eczema and osteoporosis in humans and found to be oestrogenic and has been (Ma et al. 2013) detected to have androgenic properties (Cai et al. 2019; Gee et al. 2008).

Figure 2. Triclosan containing products (Image source: Live, 2014)

1.2 Glyphosate

Glyphosate (IUPAC name: N-(phosphonomethyl)glycine) is a non-selective herbicide which belongs to organophosphate family of pesticides and used to kill weeds to improve crop production. It was first introduced in 1974 by a chemist named John E. Franz working in Monsato company under commercial name of Roundup (Bento et al. 2016; Duke 2018).

It inhibits weeds growth inhibiting enzymatic activy of enolpyruvilshikimic phosphate of shikimic acid pathway which helps in synthesis of aromatic amino acids – tryptophan, phenylalanine and tyrosine (Gimsing, Borggaard, and Bang 2004). This pathway is absent in animals and limited to only some fungi, microorganisms and plants (Saunders and Pezeshki 2015). Due to this property, glyphosate was initially supposed to be non-toxic to animals.

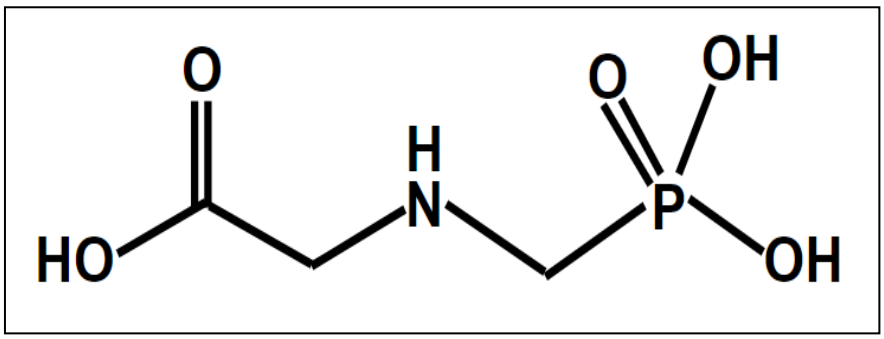

Figure 3. Chemical Structure of glyphosate

Glyphosate can bind easily to soil particles; easily biodegradable; completely soluble in water; can withstand sunlight and is very less toxic to other animals. These properties makes glyphosate an excellent herbicide (Borggaard and Gimsing 2008).

Table 2. General Properties of Glyphosate

Physical appearance	White crystalline powder
Chemical formulation	$C_3H_8NO_5P$
Mol weight	169.073 $gmol^{-1}$
Melting point	184.5˚C
Boiling point	187˚C
Density	1.704 g/cm3
Solubility	Water

Glyphosate use in agricultural and non-agricultural applications has been increased very rapidly in past 45 years (Benbrook 2016; Myers et al. 2016). Its long-term persistence in water and soil raises concerns about its long-term effect on human health (Bai and Ogbourne 2016). Glyphosate has been categorized under group of probable carcinogenic substances in 2015 report by IARC (International Agency for Research on Cancer).

1.3 Zebrafish, a vertebrate animal model

Zebrafish (Danio rerio) is a teleost (bony), freshwater fish belongs to Cyprinidae family of class Actinopterygii (ray-finned fishes). Zebrafish has been used as a vertebrate animal model in various studies. It has become a popular model organism for biological studies in recent years.

An adult zebrafish is about 2.5 to 4 cm long and demands very low maintenance. It shares many physical, morphological and genomic similarities with humans comprising the brain, intestinal system, vascular system, muscle morphology and also innate immune system. About 70% of the human genome has been found to have functional similarities with zebrafish. Major advantages include short generation time of 2-3 months, a high fecundity rate (can lay about 200-400 eggs in each mating), transparent embryos so suitable for developmental studies. It is widely used for toxicological studies, drug discovery, cancer studies, angiogenesis and other human diseases (Cai et al. 2019; Gee et al. 2008).

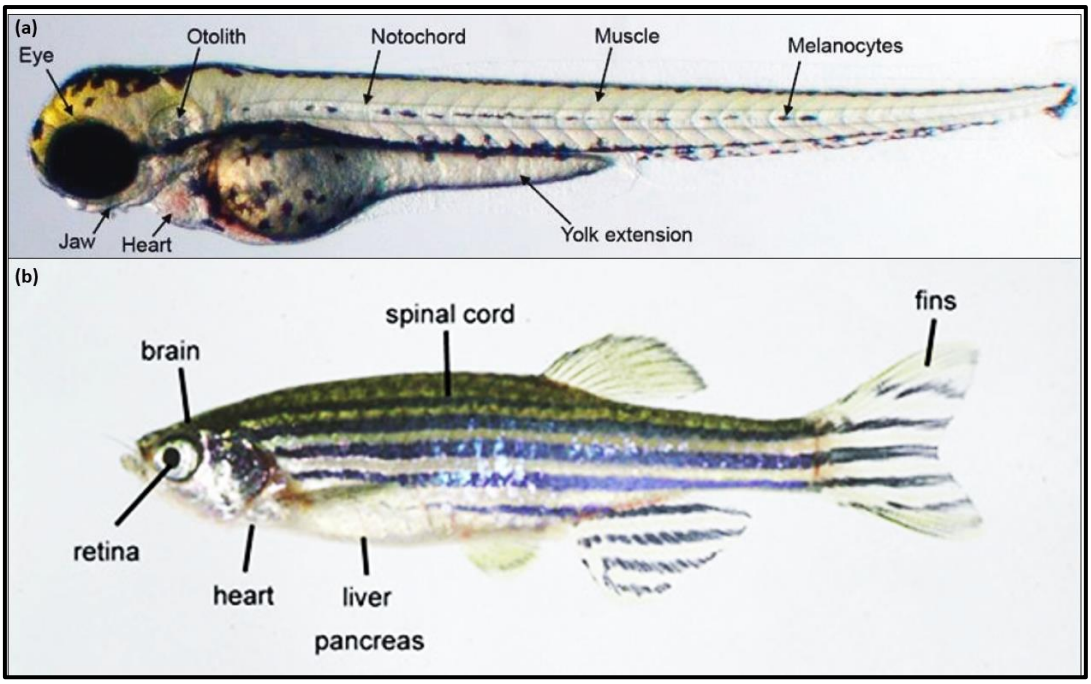

Figure 4. Morphology of Danio rerio (a) 4-dpf larvae and (b) adult zebrafish (Image source: Barrett, Chappell, Quick, & Fleming, 2006)

1.4 Developmental stage

Zebrafish has a very short generation time. It has been categorized into eight main developmental stages as shown in figure 5. In the shortest and most initial zygote period, embryo divides and acquires a 2-cell stage. Cleavage period continues until embryo reaches a 64-celled stage. In the blastula period, division continues up to 2K-cell stage and it obtains an oblong shape, leads to epiboly formation.

Gastrulation period starts in-between epiboly and continues till somites starts to form in the embryo. This is the period where germ layers rearrange themselves for correct localization of organ and tissues. Formation of tail bud and 100% epiboly mark the end of gastrulation period. Segmentation period continues from 10.33 h to 24 h. Embryo becomes more elongated and primary organs start developing and first body movement of embryo occurs in this period.

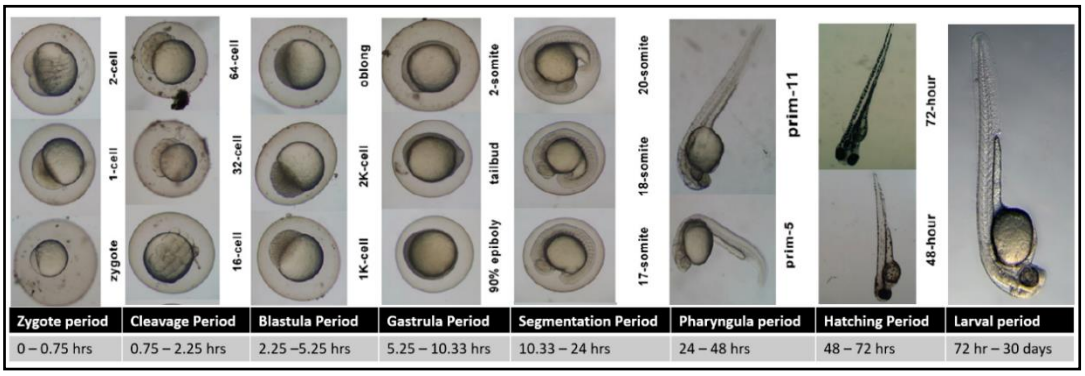

Figure 5. Development stages of zebrafish embryos
image source: (Kimmel et al. 1995)

Pharyngula period marks the circulatory system development and first heartbeat of embryo. Body axis becomes more straightened. In the hatching period, embryo comes out of its chorion layer. First bone of embryo is visible in this period. Larval period continues from 72 h to 30 days. Larva becomes sexually mature after 90 days' period.

1.5 Neuromuscular Development Morphology

Toxicology studies on zebrafish muscles are considered of very high relevance since 60% of body mass of adult zebrafish is comprised of skeletal muscles (Blagden et al. 1997). Muscle contractions are responsible for various kinds of motor behaviour such as swimming, touch-

response, tail-coiling, jerking movements etc. And perfect coordination between muscles and nervous system is what make these movements possible. Motor neurons are responsible for these kinds of motor activities. So, toxicity studies on both systems combined can help much better understanding of disease mechanisms. Skeletal muscles arise from the paraxial mesoderm and further undergoes segmentation to form somites (Devoto et al. 2006). Somites further differentiate into three sections known as dermomyotome, myotome and sclerotome. However, skeletal muscles of the trunk region and pelvic fin are present in myotome region only (Cole et al. 2011; Devoto et al. 1996).

Skeletal Muscle Cells (SMCs) originate from precursor muscle cells called adaxial cells (cuboidal shaped initially) which are formed from paraxial mesoderm (Du et al. 1997). After formation of somites, these adaxial cells elongate further to extend towards anterior-posterior axis and medial to the lateral region of somites forming a monolayer and differentiate into SMCs from 17 hpf to 23 hpf (Fox and Sanes 2007; Halpern et al. 1993). Trunk muscles of adult fish are divided into 32 segments named myotomes in the anterior-posterior axis. Every myotome consists of two kinds of muscle fibers – one is called red (slow) muscle fibers which are responsible for long period contractions and another is white (fast) muscle fibers which are responsible for sudden forceful contractions.

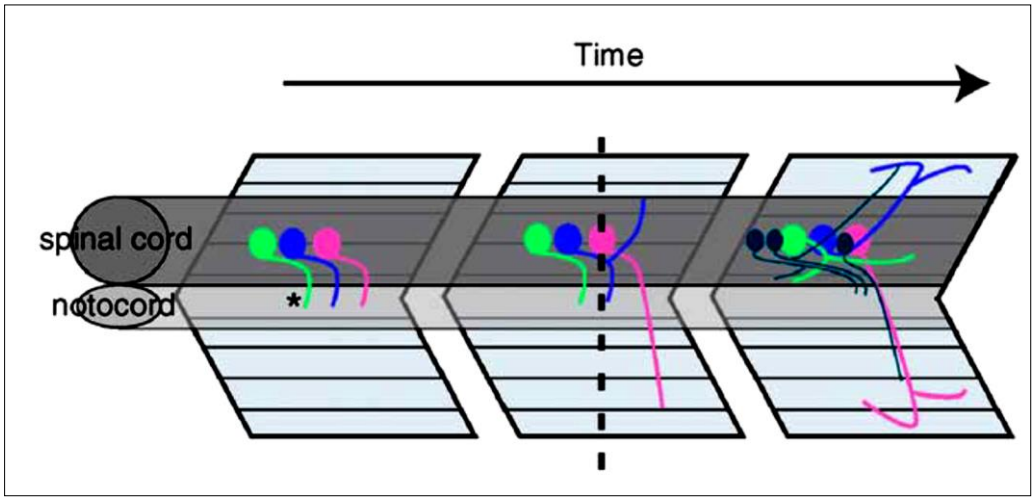

Figure 6. Primary motor neurons and their axonal growth in myotome
image source: (Panzer et al. 2005)

The first contraction happens as soon as myotome segments are innervated by the axons of caudal primary motor neurons. Three kinds of primary motor neurons are formed during

zebrafish development as shown in figure 6 represented by three different colours where pink (CaP Caudal Primary), blue (MiP Middle Primary) and green (RoP Rostral Primary) motor neurons. As development proceeds, motor neurons exit spinal cord and reach a point at horizontal myoseptum called choice point before migrating towards their destined direction in myotome. The Dorsal MiP neurons and Ventral CaP neurons extend till the edge of the myotome and then further start growing laterally. RoP extends its axon laterally in horizontal myoseptum. Please refer to figure 5 for diagrammatic visualization.

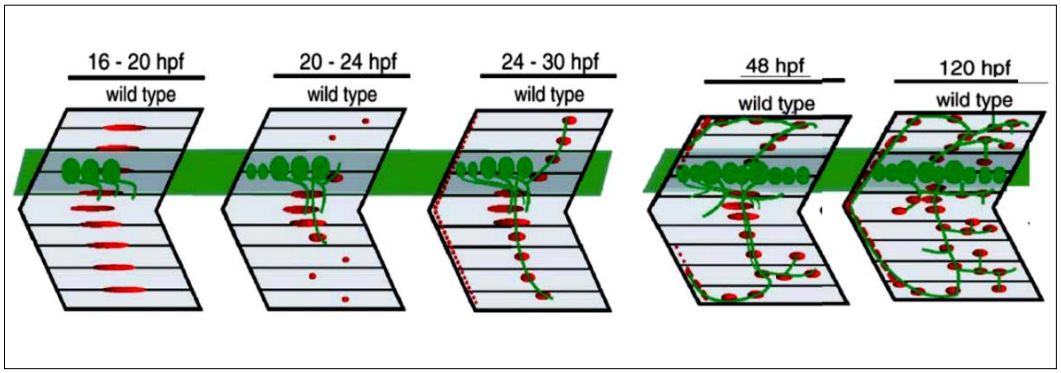

Figure 7. Motor neurons and their axonal migration myotome through 16 hpf to 120 hpf. image source: (Panzer et al. 2005)

Figure 7. illustrates how motor neurons extend their axon in a myotome through 16 hpf to 120 hpf during the development of the neuromuscular network. The Green-coloured structure refers to motor neuron cell bodies and their axons. At 16 hpf to 20 hpf primary motor neurons exit from the spinal cord through the ventral root. At 20 hpf to 24 hpf motor neurons extend toward the ventral, dorsal and middle region of myotome. From 25 hpf to 30 hpf, motor neurons reach till ventral and dorsal edge of the myotome and by 48 hpf, motor neurons turn at the edge and have extended their axons along rostro-lateral direction in myosepta and we can see axonal branches in the muscle fibers. During, 48 hpf to 72 hpf, (SMNs) Secondary Motor Neurons (SMNs) extend towards the path paved by their precursor PMNs. By 120 hpf, motor axons have extended throughout the myosepta and their axonal branches fully innervate the entire muscles of myotome. The physical connection between both types of tissue - nervous and muscle tissue is called as Neuromuscular Junction (NMJ) which ensures motor neuron-derived contractile muscle activity (Panzer et al. 2005).

1.6 Deconvolution:

Deconvolution is defined as a method to improve the quality of images by minimizing noise level through application of suitable algorithms. When we try to focus light on a specific plane of object while working with fluorescence microscope, unfocussed light from other planes - above and below the selected plane; add in to total noise level. This further gives rise to a false, low intensified blurred signal. This blurriness further cost us loss of finer structures which would otherwise be visible (Wallace, Schaefer, and Swedlow 2001).

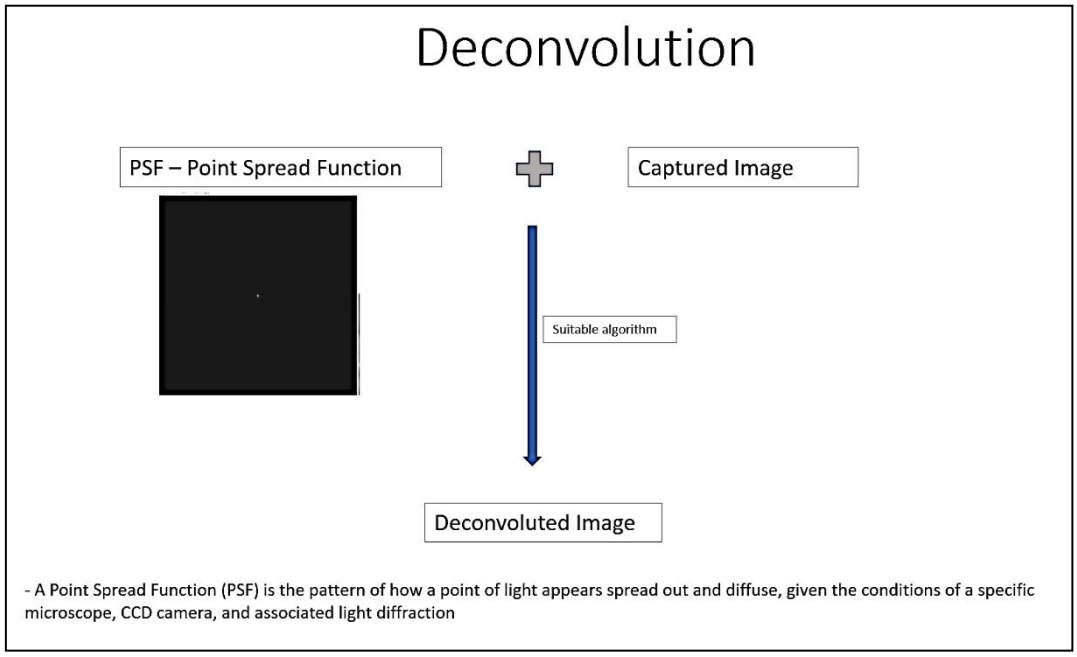

Figure 8. General idea of deconvolution

The role of a Point Spread Function (PSF) is most important while deconvolution process. It is defined as a pattern about how a light point would diffuse out under given microscopic conditions. As images consists of points only; a PSF helps us figuring out how an image should look like after removal of noise signal.

There are two kinds of deconvolution processes - 2D deconvolution and 3D deconvolution. 2D deconvolution refers to processing of a single plane image while 3D deconvolution refers to processing of a stack of images taken at different focus or multiple planes (Giannini and Giannini n.d.; Sage et al. 2017). An algorithm is applied in both cases and as a resultant, we get a new dimmed but sharp image/image stack than the unprocessed one. In

case of 3D deconvolution; resultant 3D stack can be converted into a single image with high-pitched sharpness in 3D details

2D deconvolution is more cost effective if we consider time and computational effort needed. However, most of the blurriness in images arises due to diffused light coming from multiple planes. Therefore, ultimately 3D deconvolution results in a clearer and better filtered image as compared to 2D deconvolution.

Review of Literature

2.1 Adverse effects of Triclosan

2.1.1 In humans

TCS enters human body through skin and oral cavity. Here, it undergoes through both phase I and phase II metabolism process. Chemical process like hydroxylation, glucuronidation and sulfonation make TCS a highly charged polar compound (JAMES, MARTH, and ROWLAND-FAUX 2012; Wu, Liu, and Cai 2010). Previously it was reported that TCS is harmless to humans and other animals, but its first-ever allergy response was reported in 2007 (Wu et al. 2010) TCS has been found to initiate a photochemical reaction (PACD) which leads to eczema kind of skin condition resulting in red coloured rashes on face, neck, shoulder or other exposed parts of the body. These kinds of rashes develop when a part of the body which had come in contact with TCS previously; is also exposed to sunlight on the same area (JAMES et al. 2012).

TCS has been found in many human body fluids like plasma, urine and breast milk (Calafat et al. 2008; Chu and Metcalfe 2007; Schweizer 2001; Wolff et al. 2007). A study conducted by Stockholm University in Sweden found the occurrence of TCS in 60% samples of human breast milk (Adolfsson-Erici et al. 2002). Another study conducted by the National Health and Nutrition Examination Survey (NHANES) on US population of more than 6 years of age analysed urine samples for the presence of TCS. A total of 2,517 samples were analysed out of which 74.6% of samples provided positive results for TCS presence (Calafat et al. 2008; Dhillon et al. 2015). An analysis based on NHANES survey data (2005-2010) on the US population found a connection between urinary concentration of TCS and prevalence of osteoporosis with more chances in postmenopausal women rather than in premenopausal women (Cai et al. 2019; Fiss, Rule, and Vikesland 2007). Considering the hydrophilic nature of TCS, there are high chances of its accumulation in adipose tissues.
The US EPA organization has regarded chloroform as a human carcinogen. A study conducted in 2007 (Fiss et al. 2007) suggests the involvement of triclosan in generation of chloroform and may increase chloroform formation if present in chlorine-treated water.

2.1.2 In animal models

Various animal models including rat, mice and fishes etc have been used to detect toxicity potential of TCS. The structure of TCS is very similar to thyroidal hormones and hence inhibits the thyroid hormone metabolism by interfering with its binding to specific receptors. In mice, it has been shown to cause hypothermia and an inclusive depression of central nervous system (CNS) (Miller et al. 1983). A study of TCS exposure on female and male reproductive organs in mice and rat has shown many adverse effects like decreased ovary weights (Catlin et al., 2016), an earlier age onset of puberty (Stoker, Gibson, and Zorrilla 2010), decrease in male:female sex ratio (Rodríguez & Sanchez, 2010), mitochondrial dysfunction (Ajao et al. 2015) and decreased sperm density (Kumar et al. 2009).

Long term exposure of TCS induced liver carcinoma in mice (Yueh et al., 2014). It causes adverse effects on fetus development (Kumar et al. 2009) by inhibition of estrogen sulfotransferase action in the sheep placenta. TCS exposure studies conducted on transgenic zebrafish resulted in cardiac toxicity (Saley et al. 2016); developmental effects like a decrease in hatching rate, increased mortality rate (Kim et al. 2018); reduced body length, head size, eye size (Kim et al. 2018); neurotoxicity (Falisse, Voisin, and Silvestre 2017) such as increased apoptosis in CNS (Kim et al. 2018); decrease in axon length (Kim et al. 2018) and synapse density (Kim et al. 2018); also increases stress response and oxidative stress in zebrafish larvae (Falisse et al. 2017). TCS also interferes with Ca^{2+} signaling during skeletal muscle development in the early developmental stages of zebrafish (Ma, Liu, and Yu 2019).

2.1.3 Cell lines

Oestrogenic and androgenic properties of TCS has been detected in MCF7 human breast cancer cell lines and D115 A+ mouse mammary tumor cell lines (Gee et al. 2008). TCS decreased cell viability of rat neural stem cell lines in a concentration-dependent manner by augmenting ROS production and increases apoptosis in neural cells (Chaudhari et al. 2018). Human-induced pluripotent stem cell-derived cardiomyocytes undergo arrhythmic beating and downregulated homeostatic genes on exposure to TCS (Weatherly et al. 2016). TCS acts as a mitochondrial uncoupler via changing its ultrastructure, causing alteration in membrane potential and enforcing fission mechanism (Weatherly et al. 2018). TCS is 60-times more effective than another banned uncoupler named 2,4-dinitrophenol in RBL cells

and primary human keratinocytes (Weatherly et al. 2018). Both disrupt ATP production in rat basophilic leukaemia cells with TCS having an EC_{50} value of 7.5-9.7 μM as compared to 2,4-dinitrophenol with an EC_{50} value (389-677) μM.

2.1.4 Triclosan and neurotoxicity

Triclosan also causes adverse toxic effects on the nervous system. It initiates and aggravates apoptosis (Kim et al. 2018) in CNS (Central Nervous System). It also has been shown to decrease axonal branching, length and synapse density of motor neurons during the early development in Zebrafish.

2.1.5 Triclosan and muscular dysfunction

TCS also interferes with Ca^{2+} signalling during the skeletal muscle development in the early developmental stages of zebrafish (Heath et al. 2000).

2.2 Adverse effects of Glyphosate

2.2.1 In humans

The chemical structure of glyphosate consists of a phosphono-methyl and an amino acid glycine (Li et al. 2013). Commercial herbicide of glyphosate consists of surfactants such as Polyoxyetyleneamine (POEA), and various salts modifications. The surfactant helps better penetration of glyphosate in target plants. However, POEA surfactant which is used in Roundup is found to be more toxic than other surfactants used in other herbicide formulations (Carpenter, Monks, and Nelson 2016; Mesnage, Bernay, and Séralini 2013).

Increased daily intake of glyphosate by humans has been found to be associated with occurrence of anxiety, oxidative stress, kidney and liver damages even if consumed under the regulatory limits (Mesnage et al. 2015; Myers et al. 2016). A variety of human diseases such as kidney damage, liver damage, Parkinson's disease, Alzheimer's disease, autism, cancer, ADHD (Attention deficit hyperactivity disorder), reproduction diseases have been found to be associated with Glyphosate-based herbicides (GBHs) exposure (Fluegge and Fluegge 2015; Fortes et al. 2016; Mesnage et al. 2013; Mink et al. 2012; Myers et al. 2016; Swanson et al. 2014). Glyphosate and its metabolites have been found to be present in human urine and other body fluids (Krüger et al. 2014; Niemann et al. 2015).

IARC (International Agency for Research on Cancer) in 2015 categorized glyphosate as a likely potential human carcinogen. However, European Food Safety Authority (EFSA) declared glyphosate as non-carcinogenic chemical based on a report from Federal German Institute of risk management (Landrigan and Belpoggi 2018). WHO also declared Glyphosate as a non-carcinogen agent in 2017. In 2018, IARC confirmed its glyphosate-2015 report in response to criticisms by various sources(Agostini et al. 2020; Meftaul et al. 2020). These reports raise an uncertainty about carcinogenic effects of glyphosate on human health.

2.2.2 In animal model

Various animal models have been used to detect the toxicity potential of glyphosate including rat, mouse and fishes etc. Chronic and sub-chronic exposure to glyphosate

resulted in anxiety, depression, weight increase and abnormal locomotion behaviour in mouse models (Ait Bali, Ba-Mhamed, and Bennis 2017). In zebrafish models, glyphosate results in decreased heartbeat, reduced eye size, neurotoxicity, reduced gene expression in brain and eye, increased ROS production, decreased CA activity, cellular apoptosis, body malformations, elevated locomotion, cardiotoxicity, interferes NO and calcium signalling (Gaur and Bhargava 2019; Schweizer et al. 2019; Sulukan et al. 2017; Zhang et al. 2017). Glyphosate exposure increase ROS production , DNA-DSBs, abnormal spindle morphology in mouse oocytes (Zhang, Xu, and Feng 2019).

2.2.3 In cell lines

Glyphosate has been found to produce estrogenic and anti-estrogenic effects such as in protein expression of ERα and ERβ receptor and increased proliferation in human breast cancer cell lines T47D (Mesnage et al. 2017; Sritana et al. 2018; Thongprakaisang et al. 2013). Glyphosate exposure induces cell proliferation, imbalances [Ca^{2+}] levels and increases ROS generation in human skin keratinocyte cells (George and Shukla 2013). Acute exposure of glyphosate also increases permeability of blood-brain barrier (Martinez and Al-Ahmad 2019). A study on Roundup exposure in human placental cell lines showed less cell viability and found to be two-times effective than glyphosate alone (Richard et al. 2005). GBH exposure on HEK 293 cells caused total cell death after 24 h exposure due to reduced mitochondrial enzyme activity and induction of apoptosis by caspase 3/7 activation (Benachour and Séralini 2009).

Scope of the study

3.1 Aim

TCS and glyphosate are two common chemicals that have emerged as pollutants. In this project, the effects of TCS and Glyphosate have been observed on zebrafish embryos when the embryos were exposed to the above said chemicals individually or in combination.

We also examined neuromuscular abnormalities in zebrafish embryos treated with TCS by labelling embryos with *znp-1* primary antibody which is a PMN axon marker. The anti-*znp1* antibody detects a form of synaptotagmin 2 which is present in primary motor neurons of zebrafish embryo (Fox and Sanes 2007)

3.2 Objectives

3.2.1 To observe and compare toxicity of TCS and Glyphosate (Combined v/s Single exposure)

- Mortality and hatching rate
- Morphological abnormalities/deformations such as yolk sac edema, pericardial edema, deformed spinal curvature, tail bending, body malformations
- Larval length

3.2.2 To observe effect of TCS on neuromuscular properties of larva after 96 h exposure

- To detect any change in chevron angle due to TCS treatment
- To check any irregularity in Neuromuscular Junction (NMJ) due to TCS treatment

Materials and Methods

4.1 Zebrafish Housing

Zebrafishes were acquired from a local vendor and maintained in rectangular tanks (10 L and 6 L) containing reverse-osmosis (RO) water for about four weeks to make them accustomed to the lab environment. Electric heaters and air bubble stones were used to maintain temperature and dissolved oxygen levels of water in tanks respectively. The water of tanks was changed on alternative days. Fishes were fed twice daily with commercially available fish food. After the adaptation period, fishes were transferred to automatic e-Rack, a specialized recirculatory system for zebrafish housing.

4.2 Zebrafish mating

Zebrafish mating is performed in specially designed mating chambers. It consists of two rectangular boxes – one smaller box (upper chamber) having hollow mesh bottom and can be kept inside the bigger box. Embryos can pass through the hollow bottom while fishes would remain in the upper chamber. One male fish and two female fishes were separated by a glass plate and kept in the chamber for 12 h of dark condition. The next day, glass plate was removed, and fishes were allowed for spawning under light condition for 1.5 h. After fertilization, embryos were collected in 90-mm petri plate with Pasteur pipette. Embryo were first washed and cleaned carefully to get rid of any debris or faeces materials. Final wash of embryos was done with 1X E3 medium for two times. Then embryos were counted and placed in E3 medium in a 90mm petri plate. Lastly, embryos were placed in an incubator set at temperature of 28 ±1˚C for 5 h before the start of drug exposure.

4.3 Preparation of solution

4.3.1 Preparation of E3 Medium

Table 3. Preparation of stock E3 medium (60x)

Chemicals	**Amt taken (g)**	**RO water added**	**Final Conc^{n}**
NaCl	8.7	Set pH to 7.2 and make final volume 250 ml.	60x E3
KCl	0.4		
$CaCl_2.2H_2O$	1.45		
$MgCl_2.6H_2O$	2.44		

Table 4. Preparation of working E3 medium (1x)

Stock Sol^{n} (60x) (ml)	**RO water (ml)**	**Final volume (ml)**	**Final Conc^{n}**
10	590	600	1x E3

4.3.2 Preparation of TCS Solution

Triclosan was purchased from Sigma Aldrich (PHR-1338). For preparation of stock solution I, we dissolved 14 mg of Triclosan in 1.4 ml of acetone solution and then mixed properly. Stock solution was stored at 4˚C. The table below provides the details of preparation of the both stock and working solutions.

Table 5. Preparation of stock TCS solution I

Conc^{n} needed (mg/ml)	**TCS (mg)**	**Volume of acetone**	**Final Conc^{n}**
10	10	1ml	10 mg/ml

Table 6. Preparation of stock TCS solution II

Conc^{n} needed (mg/ml)	**stock I soln (µl)**	**E3 medium (ml)**	**Final volume (ml)**
0.1	100	9.9	10

Table 7. Preparation of TCS working solution

Conc^{n} Required (µg/ml)	Stock II solution (µl)	E3 medium (ml)	Final volume (ml)
0.3	3	0.997	1
0.6	6	0.994	1
0.3	75	24.925	25
0.6	150	24.850	25

4.3.3 Preparation of Glyphosate solution

Glyphosate was purchased from Sigma Aldrich (45521). For preparation of stock solution, we dissolved 50 mg of Glyphosate in 10 ml of E3 solution and then mixed properly. Stock solution was stored at 4˚C. The table below provides the details of preparation of the both stock and working solutions.

Table 8. Preparation of stock Glyphosate solution

Conc^{n} needed (mg/ml)	Glyphosate (mg)	Volume of E3	Final Conc^{n}
50	50	10 ml	5 mg/ml

Table 9. Preparation of working Glyphosate solution

Conc^{n} needed (µg/ml)	Vol. of stock I (µl)	Volume of E3 (ml)	Final Conc^{n}
50	10	990	50 µg/ml
100	20	980	100 µg/ml

4.3.4 Preparation of (acetone) solvent control solution

Table 10. Preparation of Stock Acetone (solvent control) solution

Conc^{n} Required (ml/ml)	Acetone stock solution (µl)	E3 medium (ml)	Final volume (ml)
0.01 ml/ml	100	9.9	10

Table 11. Preparation of solvent control (acetone) working solution

Conc^{n} Required (ml/L)	Stock solution (µl)	E3 medium (ml)	Final volume (ml)
0.6 ml	6	0.994	1
0.6	150	24.850	25

4.3.5 Preparation of PBS (Phosphate Buffer Saline) solution

Table 12. Preparation of PBS working solution

Chemicals	Amt taken (g)	E3 solution	Final Conc^{n}
NaCl	4.0	Set pH to 7.2 and make final volume 500 ml.	1x PBS
Na_2HPO_4	0.72		
KH_2PO_4	0.12		
KCl	0.1		

4.3.6 Preparation of Depigmentation solution

Table 13. Preparation of depigmentation solution

Chemicals	Volume taken (ml)	Final volume (ml)
30% H_2O_2	0.5	10 ml
5% KOH	1.0	
Autoclaved RO water	8.5	

4.3.7 Preparation of blocking solution

Table 14. Preparation of blocking solution

Chemicals	Volume taken (ml)	Total volume (ml)
BSA (Bovine Serum Albumin)	0.1 g	10 ml
DMSO	0.1 ml	
1X PBS	9.9 ml	

4.3.8 Preparation of PBST solution

Table 15. Preparation of PBST solution

Chemicals	Volume taken (µl)	Final volume (ml)	Final conc^{n}
Triton X-100	20	10 ml	2x triton in PBS
1X PBS	980		

4.3.9 Preparation of formaldehyde solution

Table 16. Preparation of formaldehyde solution

Chemicals	Volume taken (ml)	Total volume (ml)	Final Conc^{n} (%)
Formaldehyde (37% w/v)	1	10 ml	4 %
1X PBS	9		

4.3.10 Preparation of mounting media (PPD Glycerol)

Table 17. Preparation of 0.1 M tris buffer

Chemicals	Volume taken	Total volume (ml)	Final Conc^{n} (M)
Tris buffer	605.7 mg	Adjust pH to 9.0 using conc. HCL	0.1 M
Autoclaved MQ water	50 ml		

Table 18. Preparation of PPD- glycerol mounting media

Chemicals	Volume	Total volume (ml)	Final Volume
(p-phenylenediamine) PPD	10 mg	10 ml	10 ml
Glycerol	5 ml		
0.1 M Tris Buffer	5 ml		

4.4 Experimental Design

Figure 9. shows a pictorial representation of experimental design used for the present study. Zebrafish eggs were collected after mating and exposed to TCS at 5 hours post fertilization in E3 water. The solutions were replaced with a fresh solution after every 24 h duration till 96 hours of TCS exposure. Hatching rate, abnormality rate, motality rate and length were calculated at the end of 48 h, 72 h, 96 h and 96 h respectively. For NMJ analysis, 96 h exposed larvae were fixed in 4% formaldehyde overnight at 4˚C before whole-mount labelling with *znp1* primary antibody. Images were captured with the Fluorescence microscope of Olympus (lX73 series) equipped with a Procam camera HS-10 MP for further analysis.

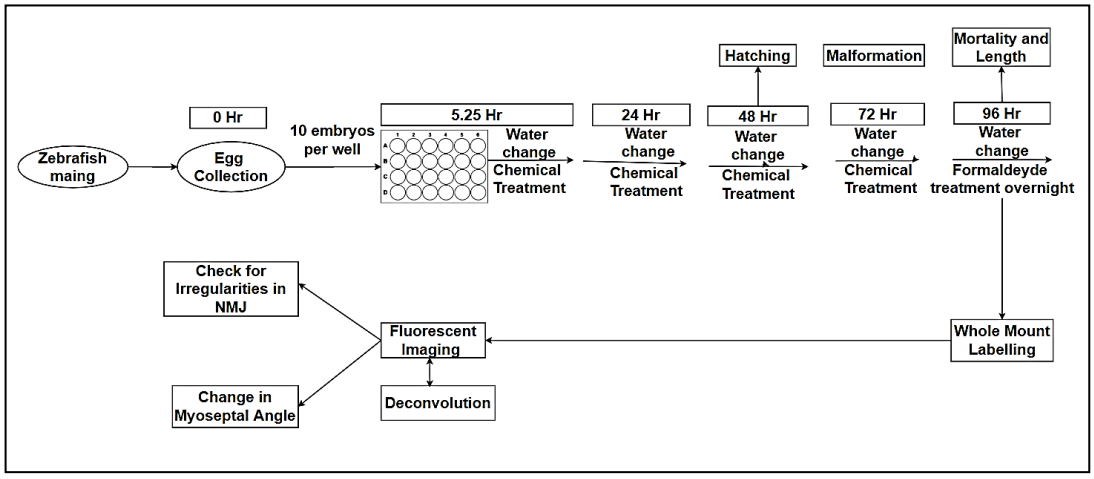

Figure 9. Experiment design

For chevron angle measurement, we selected a definite trunk region of larvae containing a total of 5 segments. Segment present just above the yolk-sac extension end was identified as

‘0’ and two adjacent consecutive segments on its either direction (both rostral and caudal) were considered as -1, -2 and +1, +2 respectively as shown in figure 10.

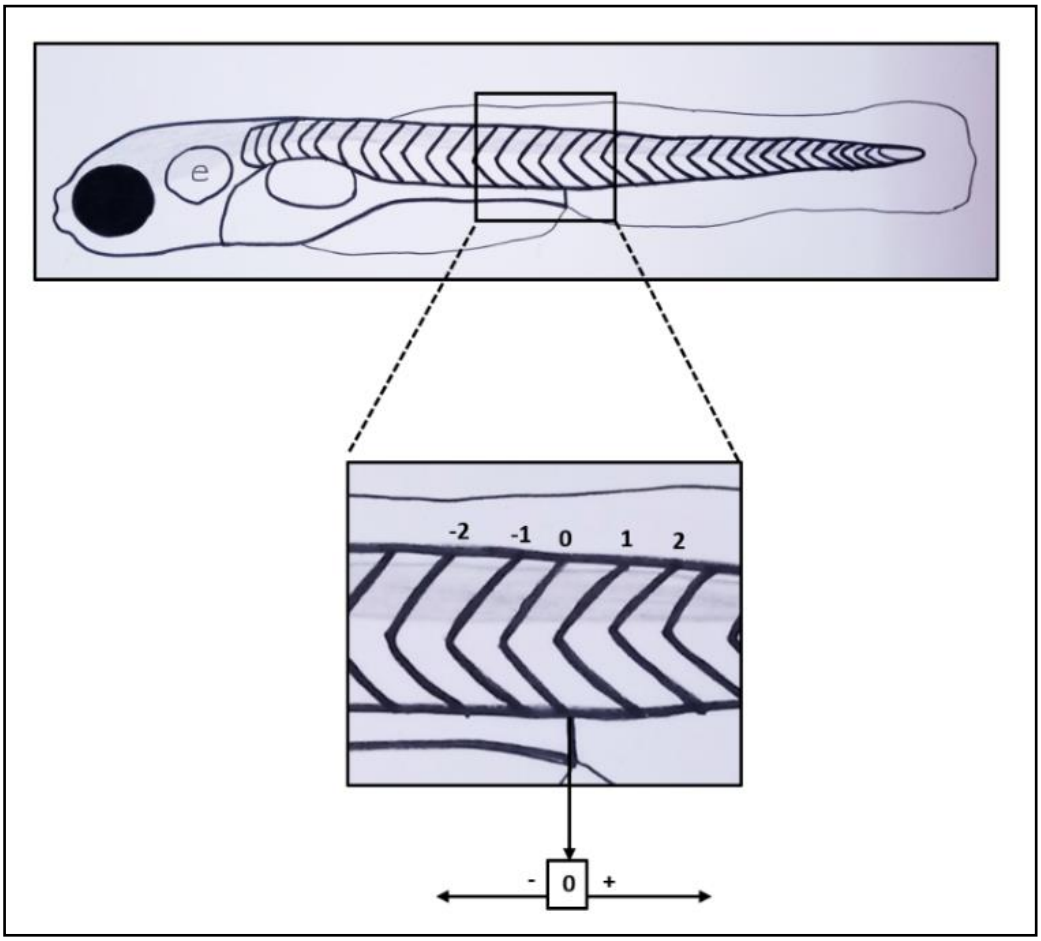

Figure 10. Larval region for angle measurement

For NMJ analysis, we selected a definite trunk region of larvae containing a total of 11 segments. Segment present just above the yolk-sac extension end was identified as ‘0’ and five adjacent consecutive segments on its either direction (both rostral and caudal) were considered as -1 to -5 and +1 to +5 respectively as shown in figure 11.

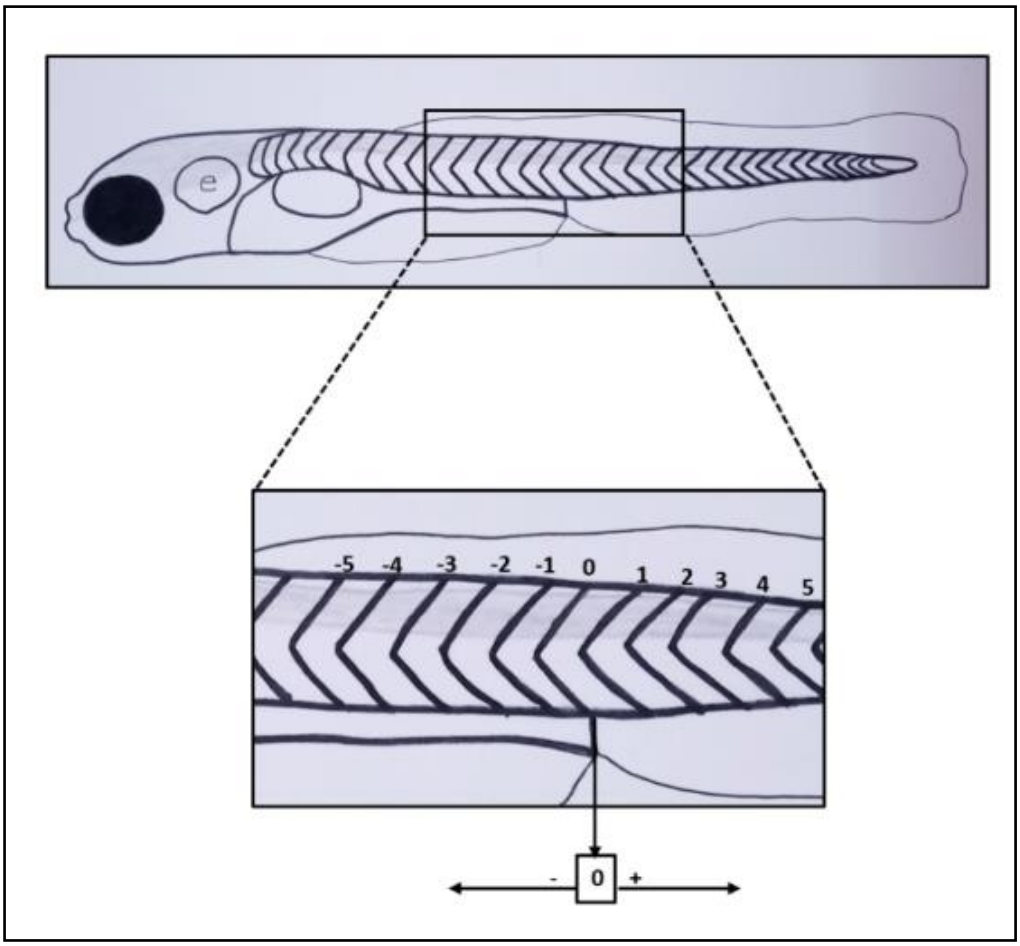

Figure 11. Larval region for discontinuity analysi

4.5 Exposure with Chemicals

After 5 h of incubation at 28±1˚C, the embryos were observed for the presence of any unfertilized/dead ones. The unfertilized/dead embryos were separated from the healthy embryos manually with help of Pasteur pipette. Then to start drug treatment, embryos were first transferred in a 24-well plate with 10 embryos in each well and exposed to respective chemical was 96 h with 1 ml of solution per well. Prior to drug treatment, we emptied E3 medium from each well and washed with corresponding chemical solution and finally kept either in E3 solution or treatment solution. Treated embryos were kept in chemical solutions and E3 medium was used as a solvent control. The solutions were replaced with fresh solution at a 24 h window and the dead embryos were removed time to time throughout the experimental period.

4.6 Mortality and Hatching rate

After every 24 h exposure, zebrafish embryos were analysed for mortality; dead larvae were removed and solutions were replaced with fresh solutions every time. This process was continued for 96 h of respective drug exposure. Finally, at the end of 96.h exposure, cumulative % mortality was calculated as follows:

% Mortality= (no of dead larva / total no of larva) *100

Hatching is a developing process in which zebrafish embryo comes out of their chorion layer. For hatching rate, zebrafish embryos were analysed for hatching after 48 h exposure; dead larvae were removed and solutions were replaced with fresh solutions every time after every 24 h. This process was continued for 48 h of drug exposure. Finally, at end of 48 h exposure period, final % hatching was calculated as follows:

% Hatching = (no of larvae hatched / total no of live larva) *100

4.7 Abnormality rate

After start of chemical treatment at 5 h post fertilization, chemical solutions were replaced with fresh solution at every 24 h window. At the end of 72 h exposure period, larvae were analysed for presence of any kind of morphological abnormalities such as TND – Tail Non-Detachment, YSE – Yolk Sac Edema, SC- Spinal curvature, PCE – Pericardial Edema, TB – Tail Bending. 5 to 15 larvae were chosen randomly from each concentration for analysis in each experiment. Experiment was repeated four times. Percent Abnormality at 72 h exposure was calculated as follows:

% Abnormality = (no of larva having any abnormality / total no of live analysed) *100

4.8 Larval length

Once the chemical treatment was started at 5 h post fertilization, chemical solutions were replaced with fresh solution at every 24 h window while removing the dead larvae every time. This process was continued for 96 h. At the end of 96 h exposure, 5 larvae from each

concentration were chosen randomly and their images were taken. The same experiment was repeated for four times. Length was measured with the help of ImageJ software.

4.9 Whole Mount Labelling

4.9.1 Materials Required:

- Acetone
- Alexa – 488 (Secondary Antibody)
- Autoclave
- Autoclaved RO water
- BSA (Bovine Serum Albumin)
- Centrifuge tubes (1.5 ml)
- DMSO (Dimethyl Sulphoxide)
- Dry water bath
- Freezer cum Refrigerator
- H_2O_2 (Hydrogen Peroxide)
- KCl (Potassium Chloride)
- KH_2PO_4 (Potassium Dihydrogen Phosphate)
- KOH (Potassium Hydroxide)
- NaCl (Sodium Chloride)
- Na_2HPO_4 (Di Sodium Hydrogen Phosphate)
- Paraformaldehyde
- pH meter
- Triton X-100
- *Znp-1* (Primary Antibody)

4.9.2 Procedure:

Fixation of zebrafish larva – After 96 h of TCS exposure, the zebrafish embryos were first washed with E3 medium twice (5 min each) then fixed with paraformaldehyde solution (4%, pH 7.2) for overnight at 4˚C.

Washing and Depigmentation - After fixation, embryos were washed with PBS (0.12 g KH_2PO_4, 0.1 g KCl, 4.0 g NaCl, 0.72 g Na_2HPO_4 in 5oo ml distilled water pH-7.4).

Depigmentation mix (0.5ml 30% H_2O_2, 1.0ml 5% KOH, 8.5ml H_2O) was added to each tube containing embryos and placed the tube under spotlight for 15 min for depigmentation.

Permeabilization - Larvae were washed with PBS (two times for 5min each) to remove the depigmentation mix followed by 20 min heat treatment in PBS at 57°C.
Permeabilization of embryos was done with chilled acetone for 5 min at -20˚ C.

Blocking - After permeabilization, larvae were washed with PBST (0.2% TritonX-100 in 1X PBS) (twice, 5 min each) and then incubated in the blocking solution (1% BSA,1% DMSO in 1X PBS) for 2 h at room temperature.

Antibody labelling – Larvae were incubated for 4 h at RT in mouse monoclonal antibody znp-1 at 1:100 dilutions in blocking solution.
After 4 h, the larvae were washed with blocking solution (twice 5 min each) and then incubated with secondary antibody (AlexaFluor-488) Thermofisher Scientifics, diluted as 1 µl in n 1 ml of blocking solution for 2 h at RT
Final washing - Final washing of labelled embryos was done with PBS (thrice, 5 min each) to remove unspecific labelling. Then, observed under a fluorescence microscope.

Note: Always have a set of larvae unlabelled with primary antibody

4.10 Imaging the embryos

For imaging purposes, we used the of inverted fluorescence microscope of Olympus (lX73 series) equipped with a Procam camera HS-10 MP. Embryos were mounted in glass-bottom dishes in mounting media containing PPD and glycerol. PPD is an anti-fade reagent.

For abnormality and length, bright field images of larvae were taken using 4x objective at a resolution of (3664*2748).

For both chevron angle and NMJ irregularities, larvae were placed under the microscope and images were captured at both 10x and 20x objective at a resolution of (3664*2748).

4.11 Deconvolution

4.11.1 Definition

Deconvolution is a method to improve images quality by minimizing noise level through application of suitable algorithms Giannini and Giannini n.d.; Sage et al. 2017; Wallace, Schaefer, and Swedlow 2001). To optimize deconvolution for our imaging system, we compared two most popular ImageJ plugin – PID and DLa2. As described in figure 12-13. Final comparison was done among three best algorithms from both plugins.

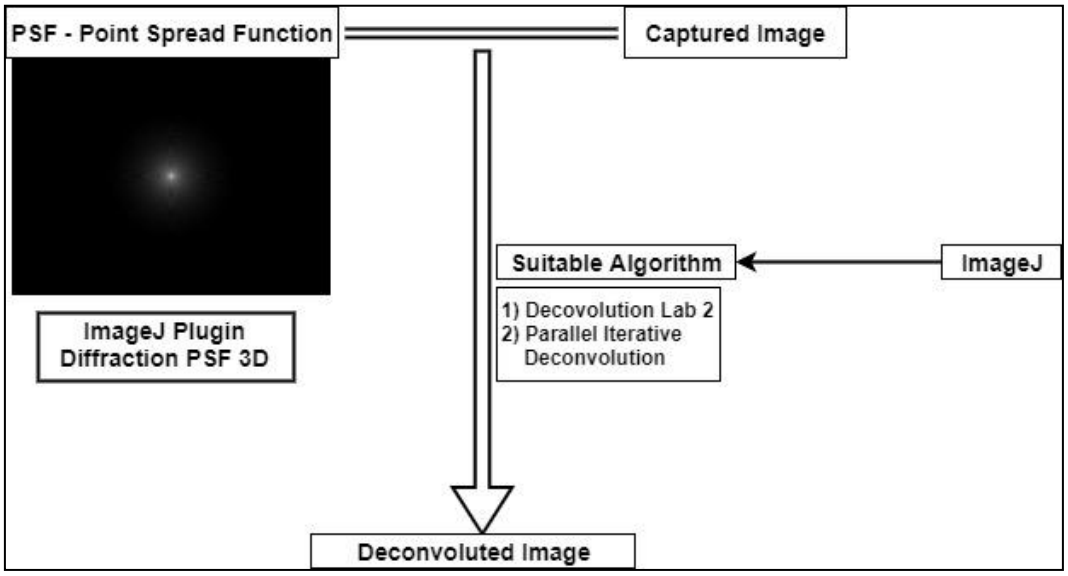

Figure 12. An overview of deconvolution optimization

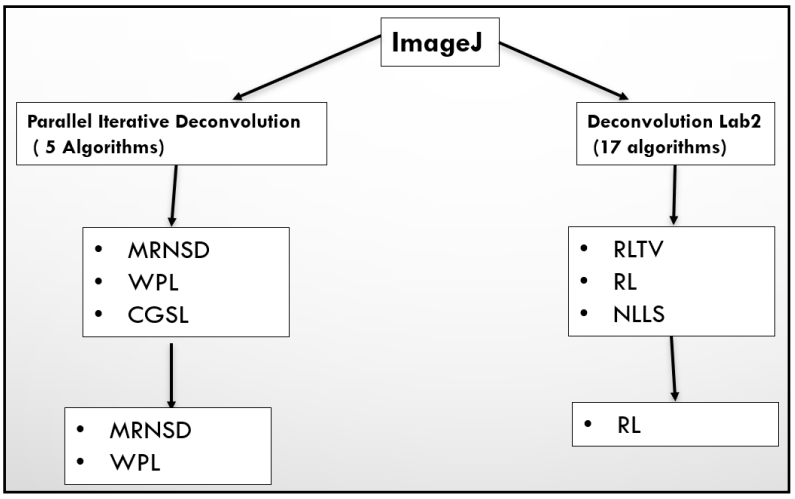

Figure 13. Final selection of best three algorithms from both plugin

Section 4.11.1 to 4.11.3 explains deconvolution process using WPL algorithm of PID plugin of ImageJ.

4.11.2 Requirements:

ImageJ software - ImageJ software is available for download at website http://ImageJ.nih.gov/ij/download.html." Save this .zip file in your desktop and extract files. A new folder having the exact name as ".zip file" will be created on desktop. Inside that folder you will find "ImageJ icon", which will launch the ImageJ application on your system. You can also pin this icon to your taskbar for easy accessibility.

Two ImageJ plugins - Now that you have installed ImageJ, you will need two plugins to download and install.

Parallel Iterative Deconvolution – This plugin can be downloaded from website https://www.softpedia.com/get/Multimedia/Graphic/Graphic-Plugins/Parallel-Iterative-Deconvolution.shtml in the form of a .zip file. Now, transfer this .zip file to the "plugins" folder of ImageJ and extract the files. Now, when you open ImageJ application, you will find this plugin already installed on plugin down menu of ImageJ as shown in figure 15.

Note: If you are unable to find PID plugin in plugin down menu, then go to "install" option on the "plugin" drop down menu of the ImageJ. This will open a New window where you "ParallelIterativeDeconvolution" folder in ImageJ plugin folder as shown in figure 15.

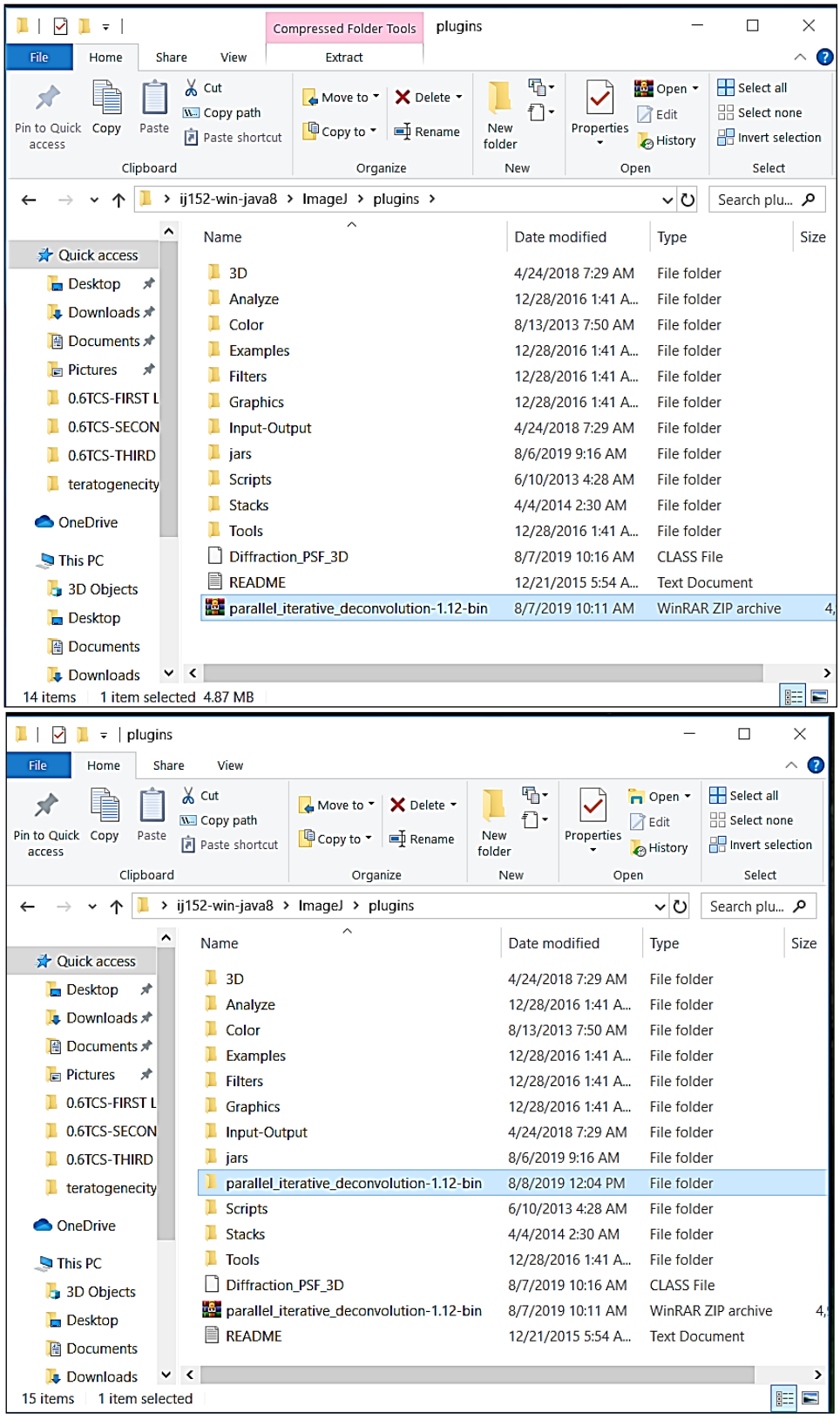

Figure. 14 (a) and (b) How to place "parallel_iterative_deconvolution-1.12.zip" file in ImageJ and extract it

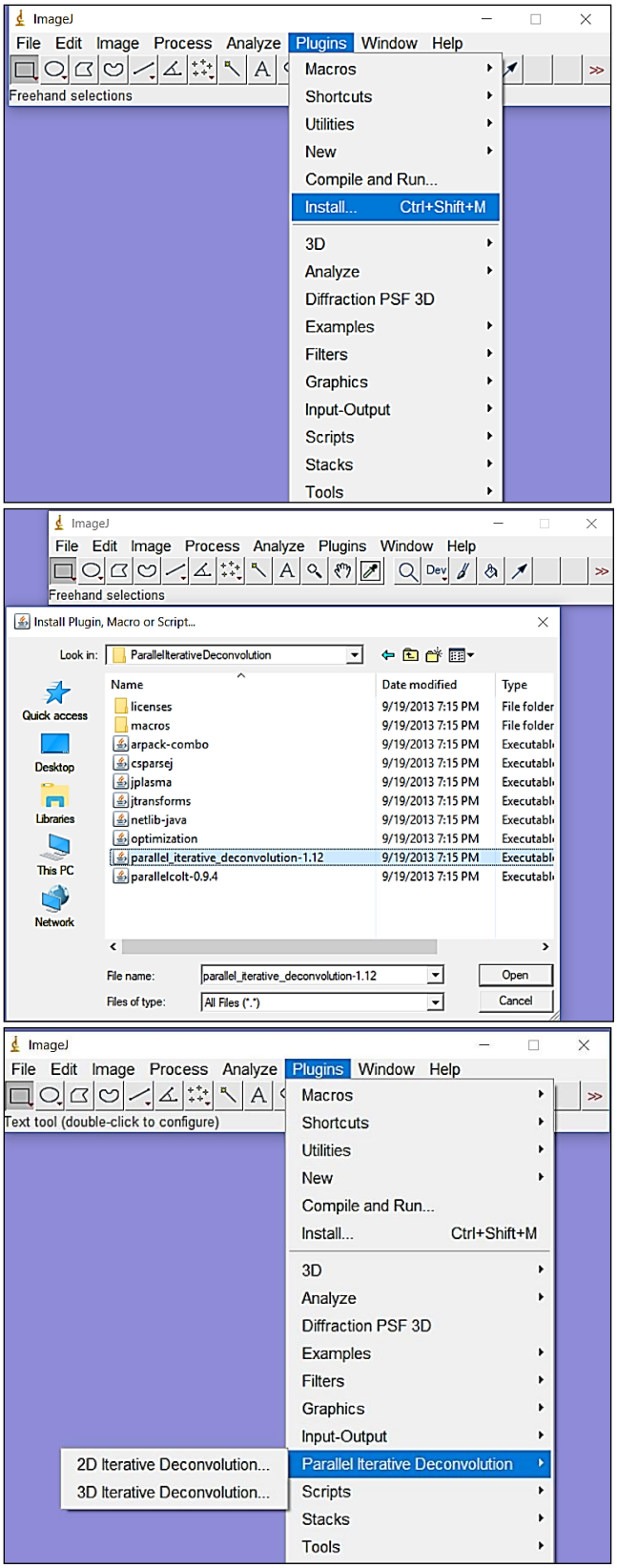

Figure 15 (a), (b) and (c) How to install "parallel iterative deconvolution" plugin in ImageJ software.

Diffraction PSF 3D - Second plugin is "Diffraction PSF 3D", download 'Diffraction_PSF_3D.class' file from website "http://fiji.sc/Diffraction_PSF_3D" and place it into the plugins folder (figure 16).

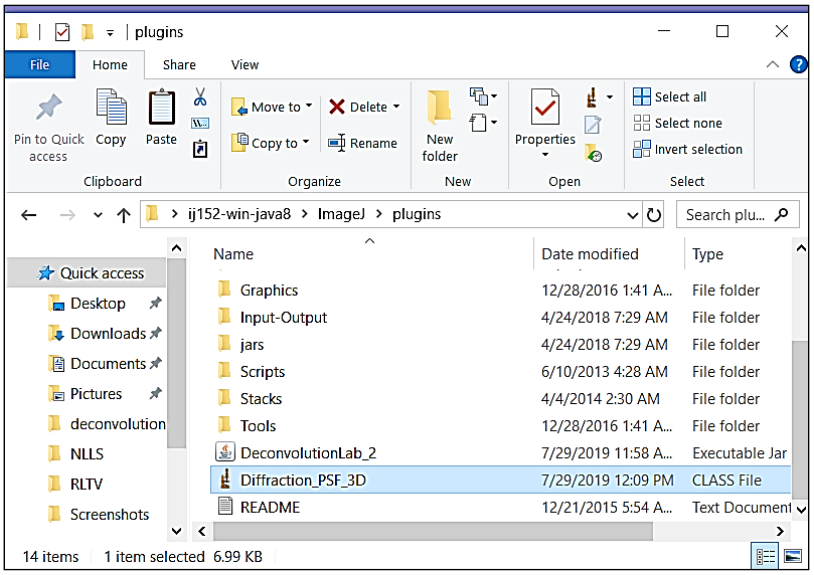

Figure 16. Diffraction_PSF_3D.class file moved to "plugin" folder of ImageJ folder.

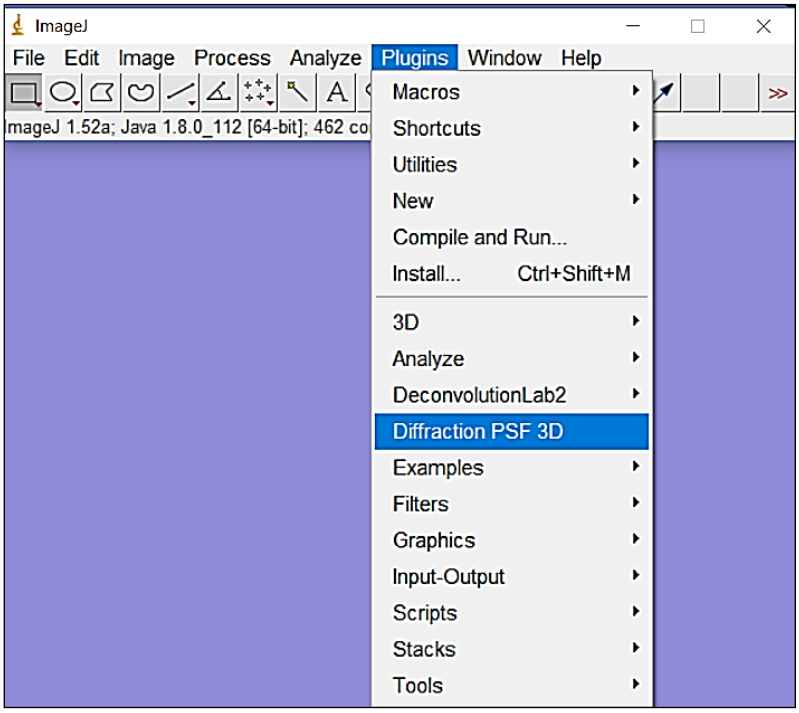

Figure 17. To check working status of plugin.

Note: Check functional status of both plugins by clicking and selecting them one-by-one to make sure it opens and works properly in your system and current version of ImageJ (figure 16). (if doesn't, exit ImageJ), delete the non-working plugin and re-download and reinstall). Repeat the whole process.

4.11.3 Creating a PSF image using Diffraction PSF 3D

As already mentioned before, Point Spread Function plays most important role in deconvolution process. It is defined as pattern how a light point would diffuse out under provided microscopic conditions. As images consists of points only; A PSF helps us figuring out how an image should look like after removal of noise signal.

Select an image – open ImageJ application. Go to "file" and then select "open". A new window will open. Select your image and enter. (figure 18-19).

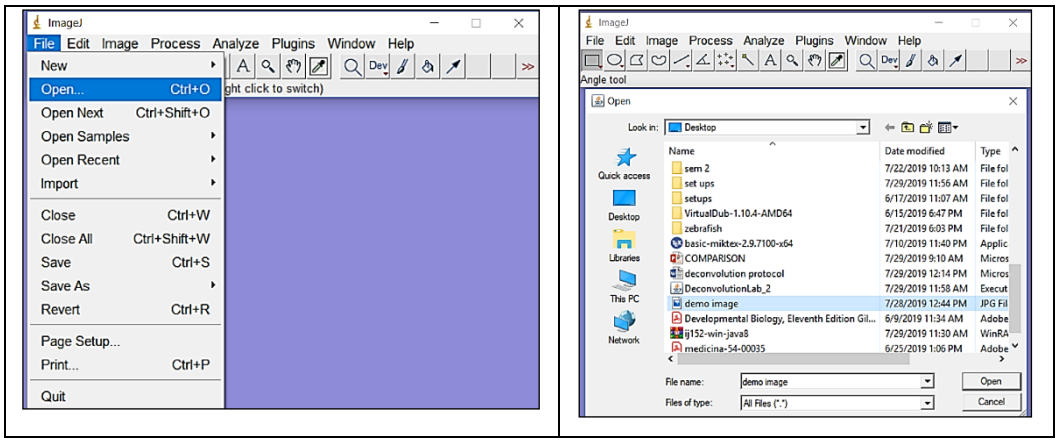

Figure 18 (a) and (b) Open an image/file in ImageJ.

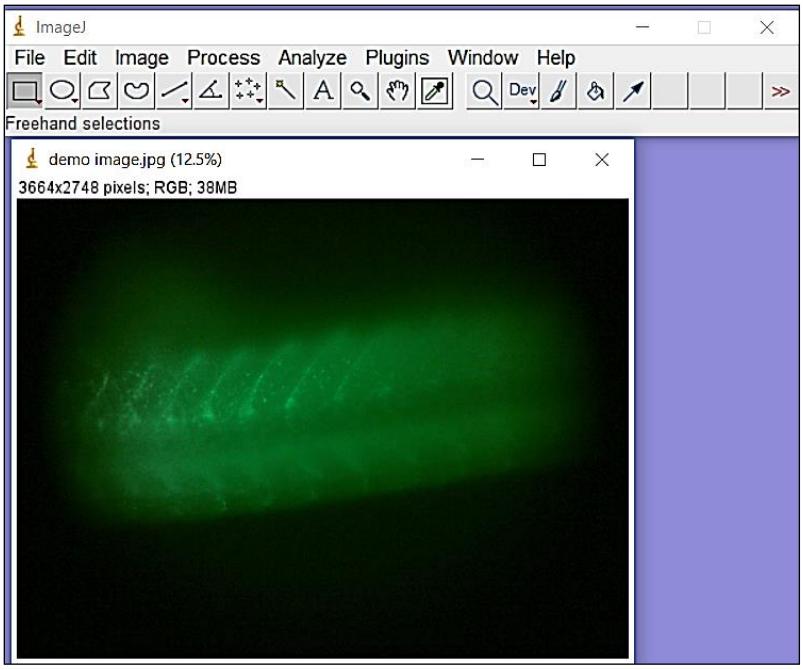

Figure 19. An image opened in ImageJ application.

Selecting criteria for PSF image – Select image window. Go to "plugins", then select "Diffraction PSF 3D", A new window with different 11 slots will open as you can see in figure 20.

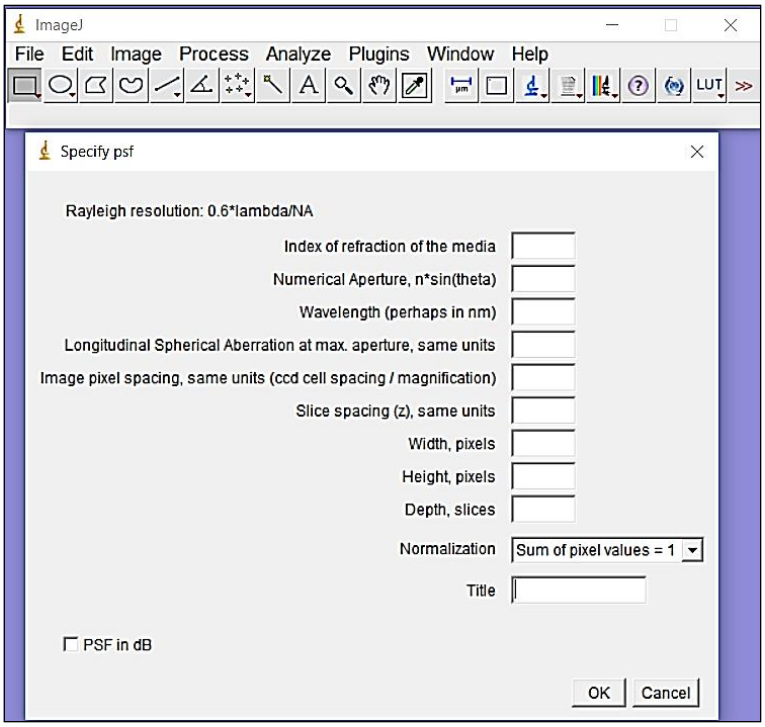

Figure 20. Specify PSF window

We need to fill all these 11 slots to create a PSF image. We will discuss about each one of them one by one.:

1. Index of refraction of the media denotes refraction index of the medium/solution, in which sample is immersed for imaging purposes. For example, if sample is dry and no immersion fluid is being used, it will be considered as air having refractive index (RI) of 1.00029. In case, you are using any kind of immersion oil or any other solution, then RI of that will be entered in the position. Usually you can find it online or imprinted on the bottle. We used glycerine as mounting media to visualize our sample then its refractive index 1.477 must be entered in the respective field.

2. Numerical aperture is a specific numerical value of any microscopic lens. It is usually imprinted upon the lens along with magnification value (figure 21). Please keep in mind that images captured via different lenses need different PSFs images for deconvolution.

Figure 21. Objective lens (10x and 20x) used in our olympus microscope

The above image shows different lens of our microscope system with 10x objective and 20x objective lens having a numerical aperture of 0.25 and 0.45 respectively. So, if we must create a psf of an image taken via 10x objective or 20x objective lens with our microscope system, we will enter numerical aperture values as 0.25 or 0.45 respectively.

3. Wavelength refers to the emission fluorescence wavelength of your fluorophore in nm. Often this value falls under 400-600 nm.
For example, if we are using alexa-488 secondary antibody for florescence visualization, so, its emission fluorescence at 515 nm, we will enter in this field.

4. Longitudinal spherical aberration is an intricate feature of a microscope and cannot be estimated comprehensively. Keeping an approximation value of 0.00 is fair and generally provides satisfied results.

5. CCD cell spacing is the most important factor among all PSF image measures. Each CCD camera has a unique pixel size (usually in micrometres) which can be found either online or in camera manual.

We used Professional Scientific ProCam HS 10MP USB CMOS camera (USB 3.0) having pixel size 1.67 x 1.67. The formula for calculating Pixel size is as followed:

$$\textbf{CCD} = \frac{pixel\ size\ x\ 1000 (to\ get\ unit\ in\ nm)}{magnification\ of\ the\ lens} = \frac{1.67\ x\ 1000}{20} = \textbf{83.5}$$

Pixel size of CCD camera is divided by the magnification of the lens used for image capturing. Our CCD camera had a pixel size of 1.67 µm x 1.67 µm and 20x lens was used for image capture; we divided 1.67 µm by 20 and got .0835 µm as a result.

Now to obtain the same unit as that of wavelength (nm) so you need to multiply this value by 1000. Then, in our case, the final CCD value we would enter in required space is 83.5 nm.

6. Slice spacing (z), same units – This value holds importance for 3D deconvolution purposes but is not useful at all in case of 2D deconvolution. So, we will simply enter its value as 0.00. It is defined as the space amid the images of the image stack in nm. For example, a photo taken at a depth of every 0.05 µm value of slice spacing would be 50 nm.

7. Width - This value should be entered in pixels. For example, if your image size is 300X500 pixel, then 300 pixels would be width of the image. Please Note if cropped image is used for deconvolution, then cropped dimensions would be considered.

8. Height - This value should be entered in pixels. For example, if your image size is 300X500 pixel, then 500 pixels would be width of the image. Please Note if cropped image is used for deconvolution, then cropped dimensions would be considered.

9. Depth, slices - This corresponds to the total number of images in image stack. In case of 2D Deconvolution, its value is entered as 1 and in case of 3D deconvolution, it is the total no of images in stack.

10. Normalization – this field area can be set at default value of '1'.

11. Title – Here, in this space, we enter the name of our PSF image. It should be matched up with the name of your given image/stack.

Note: Now if you observe "specify PSF" window carefully, you will see a check box on bottom-left corner stating as "PSF in db.". Checking this box results in a PSF obtained by plotting the sound pressure against the location. Comparison of both types of PSFs is shown in figures (22-23).

Now that we have understood how to fill this "PSF creation window", we would now enter all the values in respective areas as you can see in image

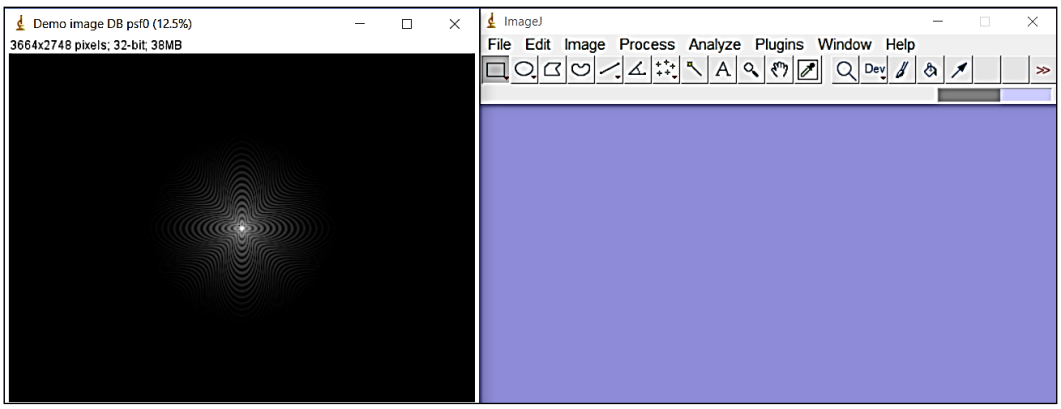

Figure 22. A psf image (in db format

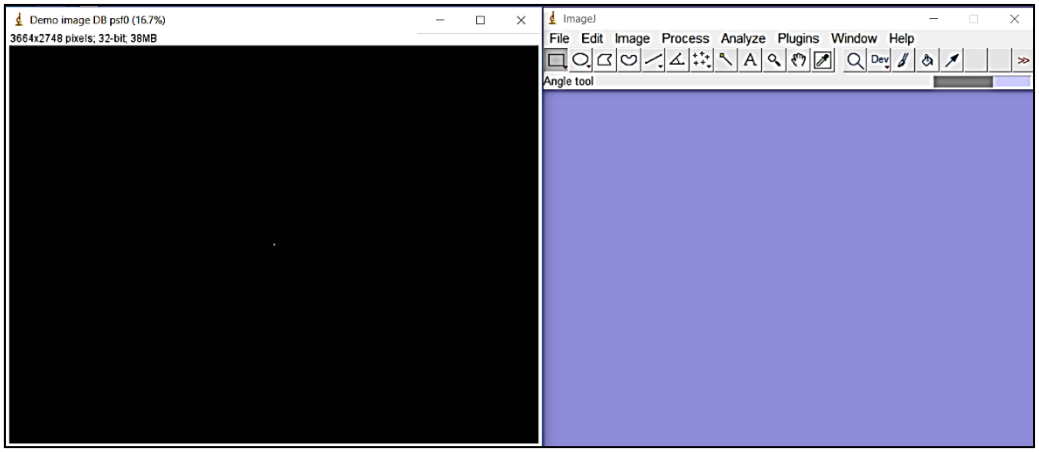

Figure 23. A psf image (not in db format)

4.11.4 STEP-BY-STEP GUIDE TO Deconvolution

This protocol delivers a demo for deconvoluting images using two plugins of ImageJ i.e. "Diffraction PSF 3D" and "Parallel Iterative Deconvolution". we are going to apply two algorithms from "parallel Iterative Deconvolution" plugin of ImageJ to deconvolute our images. Parallel Iterative Deconvolution (PID) implements a total of four iterative algorithms which are following:

- **Modified Residual Norm Steepest Descent (MRNSD)**
- **Wiener Filter Preconditioned Landweber (WPL)**
- **Conjugate Gradient for Least Squares (CGLS)**
- **Hybrid Bidiagonalization Regularization (HyBR)**

We applied all four iterative algorithms and found two of them i.e. MRNSD and WPL to be able to provide good results according to our imaging system. So, we are including only these two algorithms in this protocol.

Different steps of deconvolution

STEP 1 – Selecting an image

STEP 2—creating a PSF image using Diffraction PSF 3D plugin

STEP 3 – Splitting your colored image into channels i.e. red, green and blue

STEP 4 -- Saving each channel individually according to its respective colour

STEP 5 – Deconvolute each channel separately using deconvolution plugin with the help of PSF image

STEP 6 – Merge all deconvoluted singled channel images

4.11.4.1 STEP 1 – Selecting an image.

To select an image, go to 'file' drop down menu and select option 'open' (as demonstrated in figure 24. A new window will be opened where you select your image.

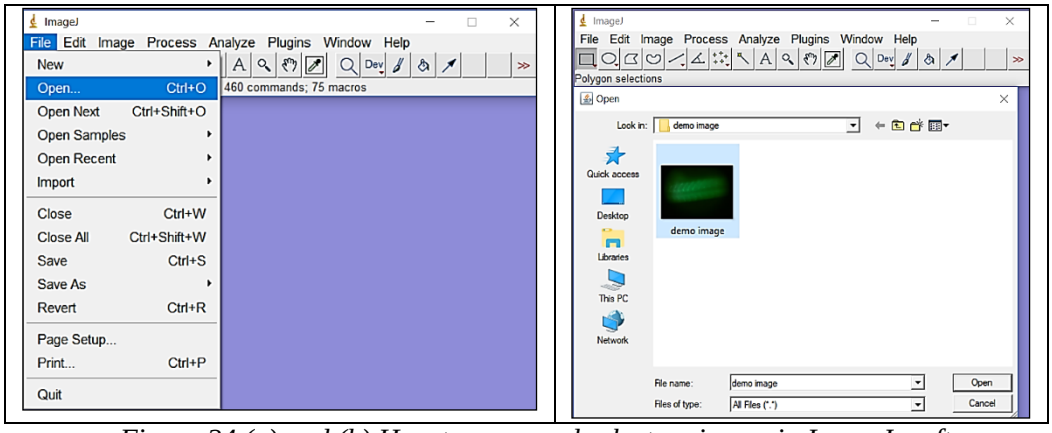

Figure 24 (a) and (b) How to open and select an image in ImageJ software

4.11.4.2 STEP 2— Creating a PSF image using Diffraction PSF 3D plugin. (Refer to figure. 18-21)

Now, you have already selected your image which you want to be deconvoluted. Go to "plugins" drop down menu of ImageJ and click on "Diffraction PSF 3D" plugin. A new window will open where you must fill some details as already described earlier.

Note: Remember to check "PSF in DB" option since we are dealing with "Parallel Iterative Deconvolution" plugin and its algorithms works well with DB-type PSF images. A new PSF image (figure. 25-28).

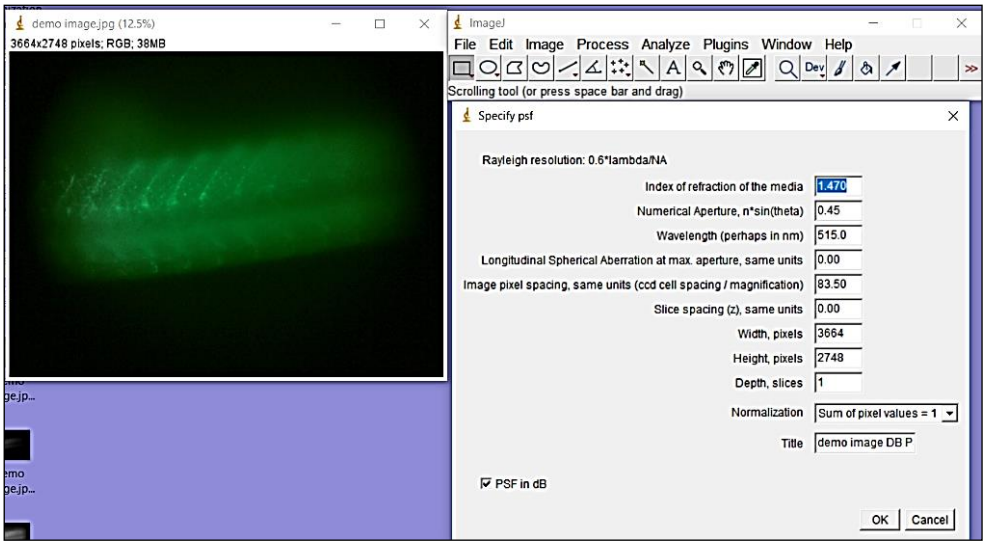

Figure 25. Filled-in "specify PSF" to get PSF image im DB format

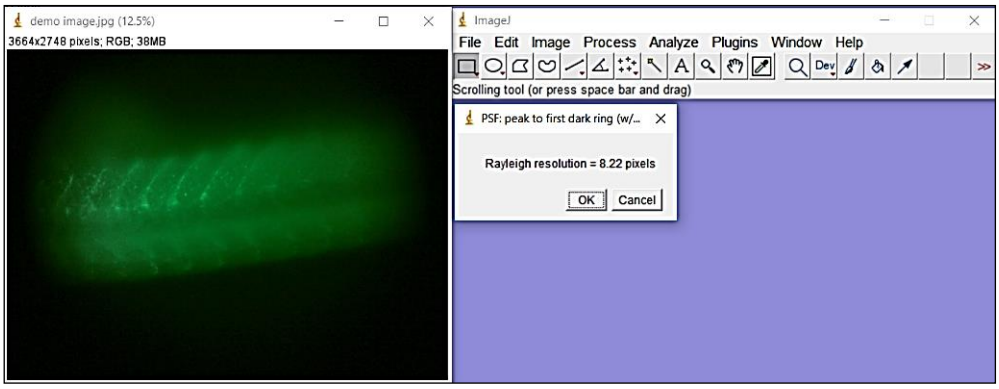

Figure 26. Rayleigh resolution

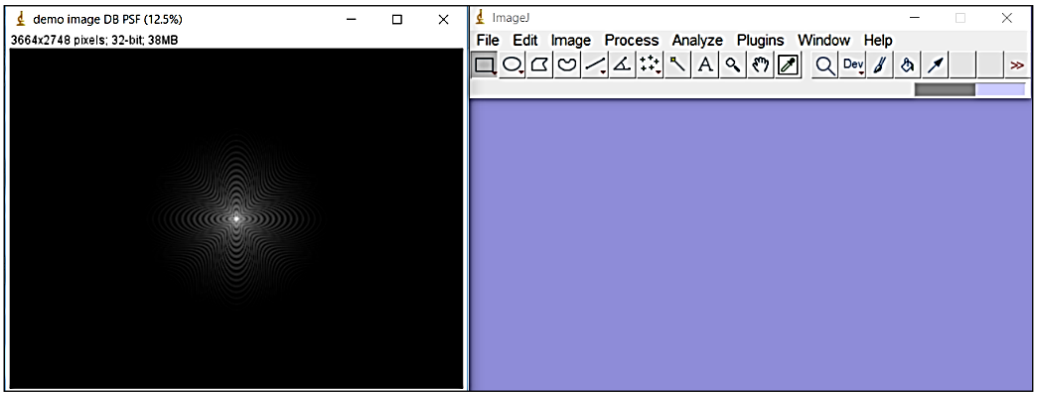

Figure 27. PSF image im DB format for our demo image

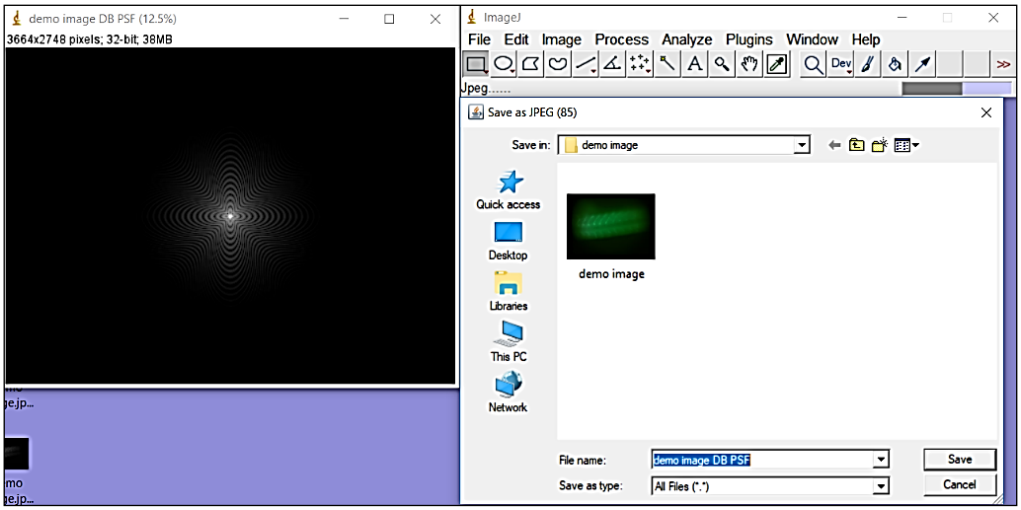

Figure 28. How to save PSF image

4.11.4.3 STEP 3 – Splitting your coloured image into channels i.e. red, green and blue.

Plugins that we use for deconvolution usually work with grey scale images, so, first we have to covert our image into grey scale image. To do that, first select your image window, go to "image" drop down menu of ImageJ and select "colour" option and then click on to "split channel" option (figure 29)

As a result, your coloured image will split into three different images indicating as 'blue channel', 'red channel' and 'green channel' as you can see in the figure 30.

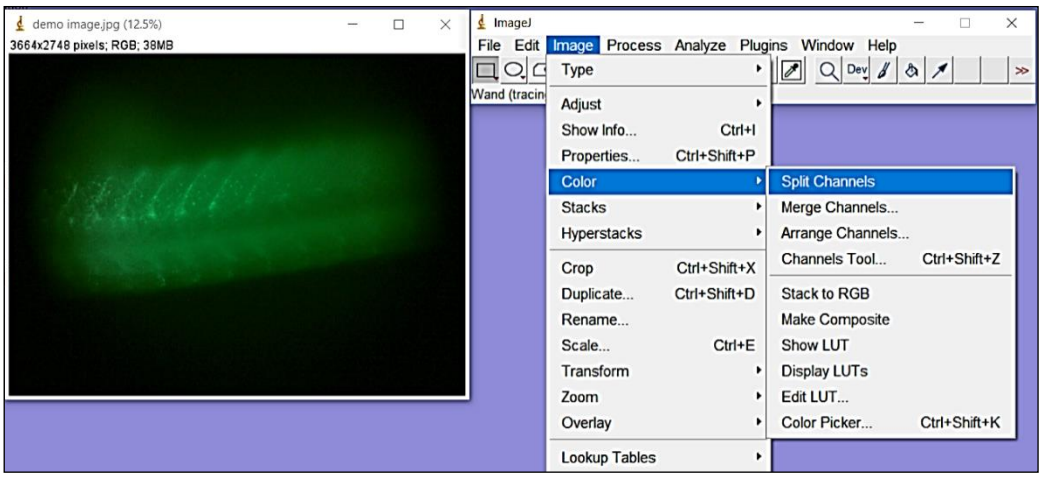

Figure 29. Conversion of coloured image to grey scale image.

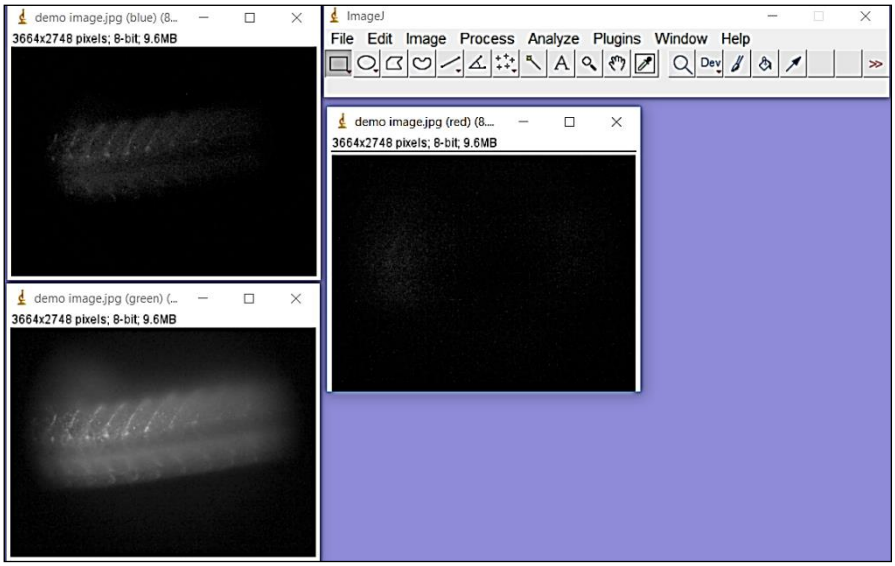

Figure 30. Splitted channel of a colored image

4.11.4.4 STEP 4 -- Saving each channel individually according to its respective colour.

Convert these split images to 8-bit if images are in some other formats and save these all three images according to their colour channels as shown in figure 31-33.

Note: If your channel images turn out to be 8-bit, then there is no need to change to 8-bit. You can directly save the images.

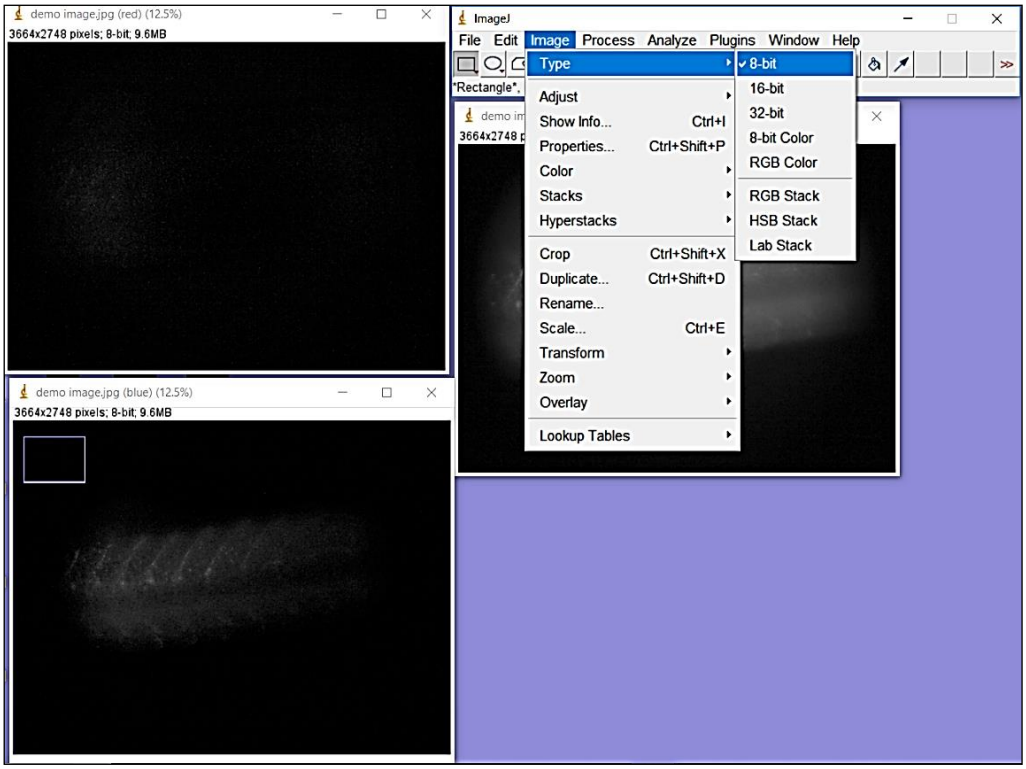

Figure 31. Changing image to 8-bit

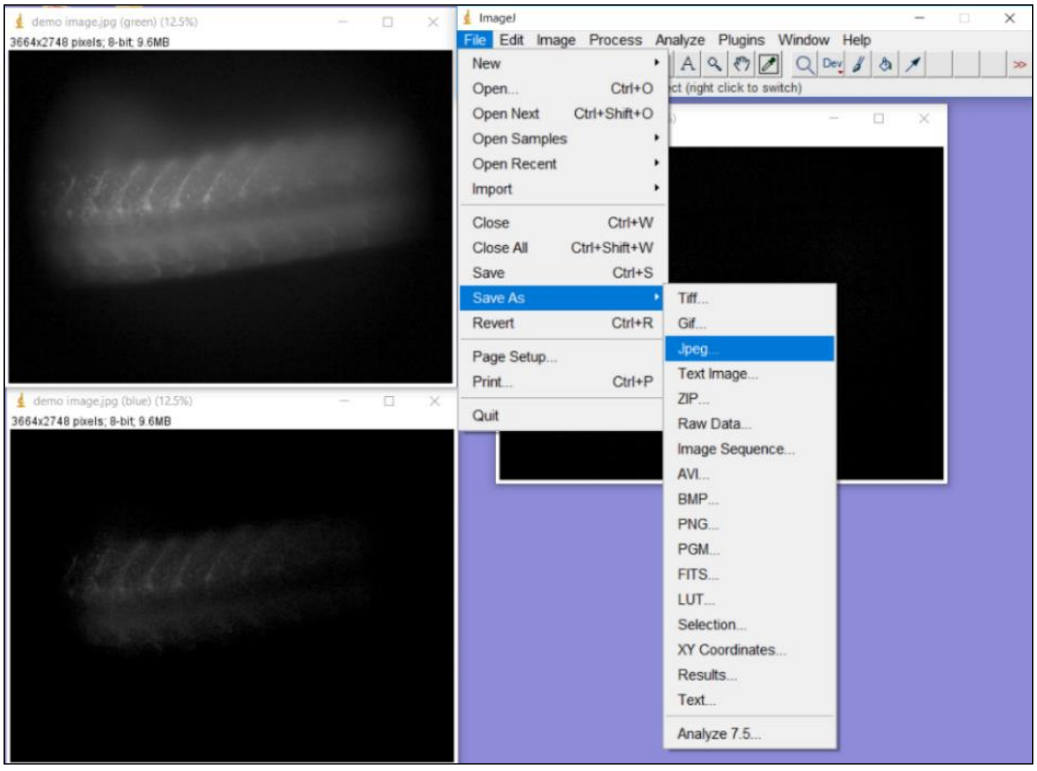

Figure 32. Saving splitted chennel of a colored image in .jpeg format

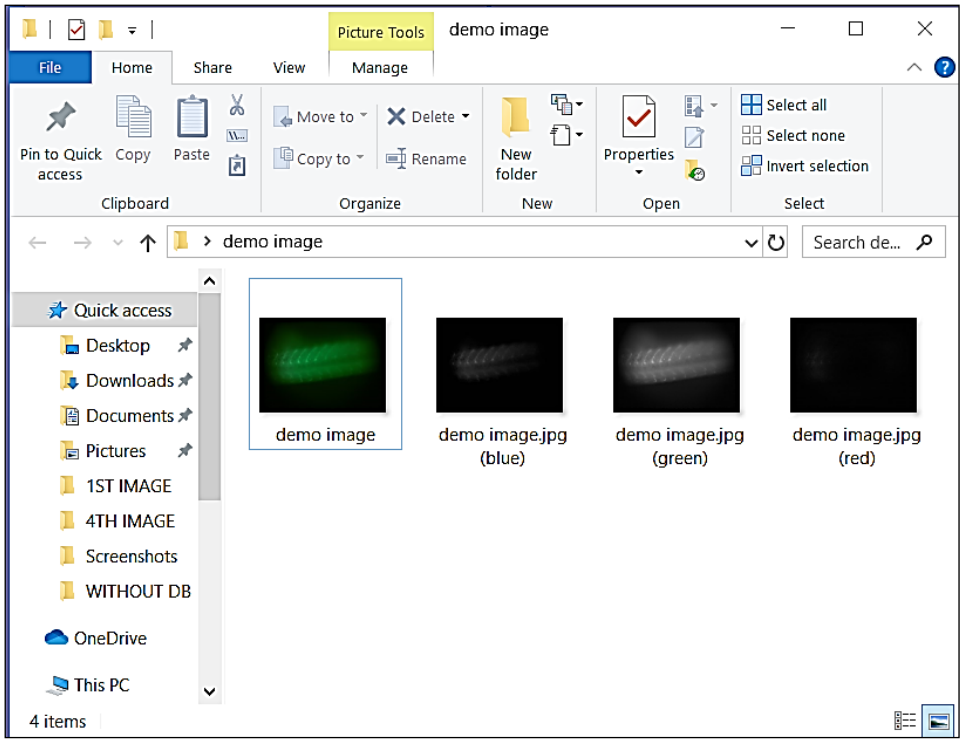

Fig 33. Saved coloured channels

4.11.4.5 STEP 5 – Deconvolute each channel separately using deconvolution plugin with the help of PSF image.

Now, the next step is to deconvolute your image with help of PSF image you got and deconvolute it with the help of an appropriate algorithm. We do this generally by deconvoluting each channel i.e. red, green and blue separately and later merging them together to get the resultant image. First, we will demonstrate MRNSD algorithm –

a) Open both your captured image and PSF (DB format) in ImageJ.
b) Go to plugin drop down menu and select “Parallel Iterative Algorithm” as shown in figure 34.

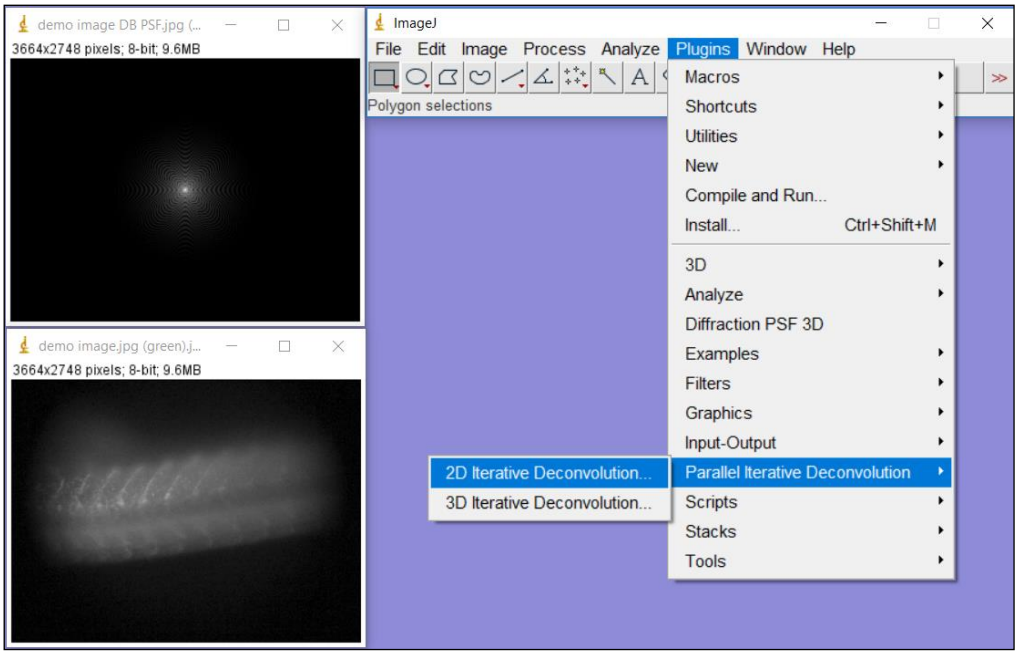

Figure 34. Illustation af point a and b in step 5 of deconvolution

c) A new window will open which contains specific place for image and PSF. Here, assigns each image its place accordingly as shown in figure 35

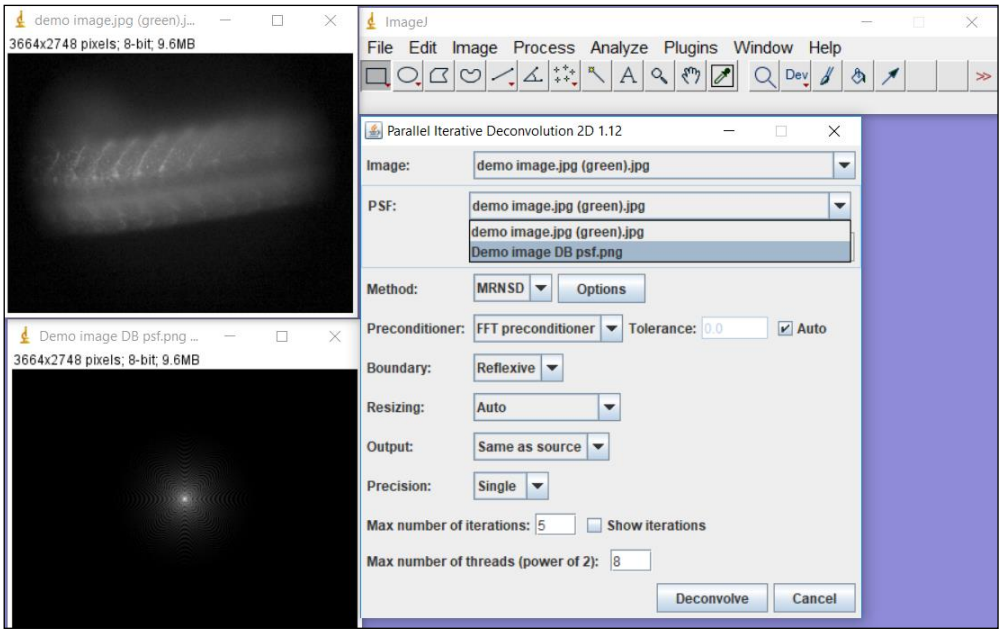

Figure 35. Assignment of each image its specific position in PID window

d) Choose MRNSD/WPL option from method drop down menu (figure 36)

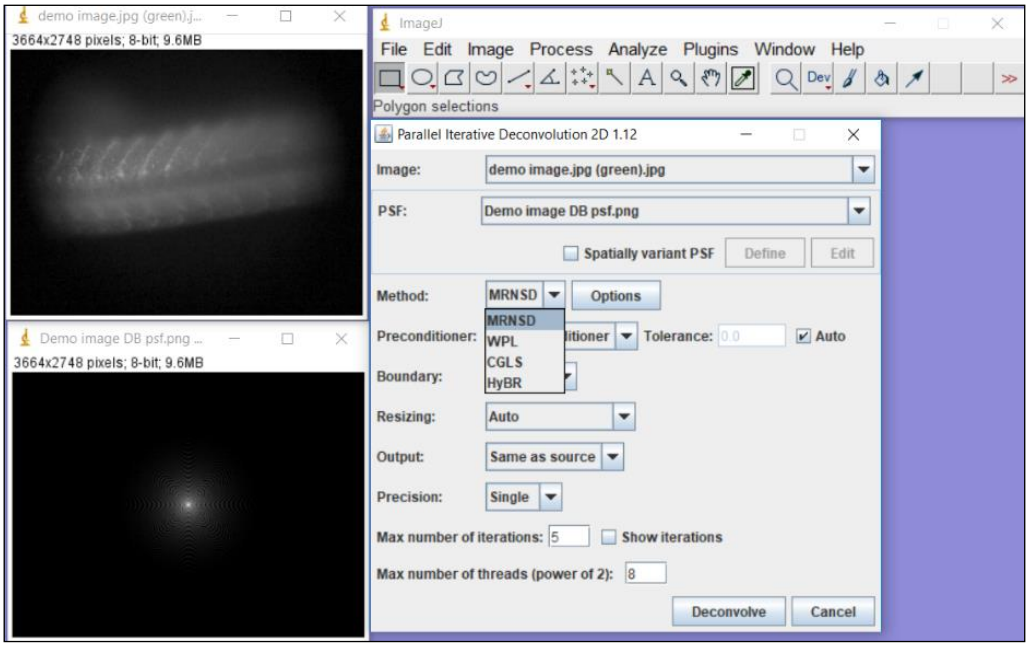

Figure 36. How to choose iterative method in PID window

e) Keep everything else as such as shown in figure 37 except max no of iteration and show iteration check box. Checking this box provides a preview of restored image after each iteration (figure 38-39). If you check this box, you can have an idea about which iteration can provide you with best results and choose accordingly. But this doesn't allow you to save images at each iteration. You can only save your image after assigned no of iterations have been finished already. Figure 39-40 show the resultant images after each iteration using PID MRNSD/PID WPL algorithm

.

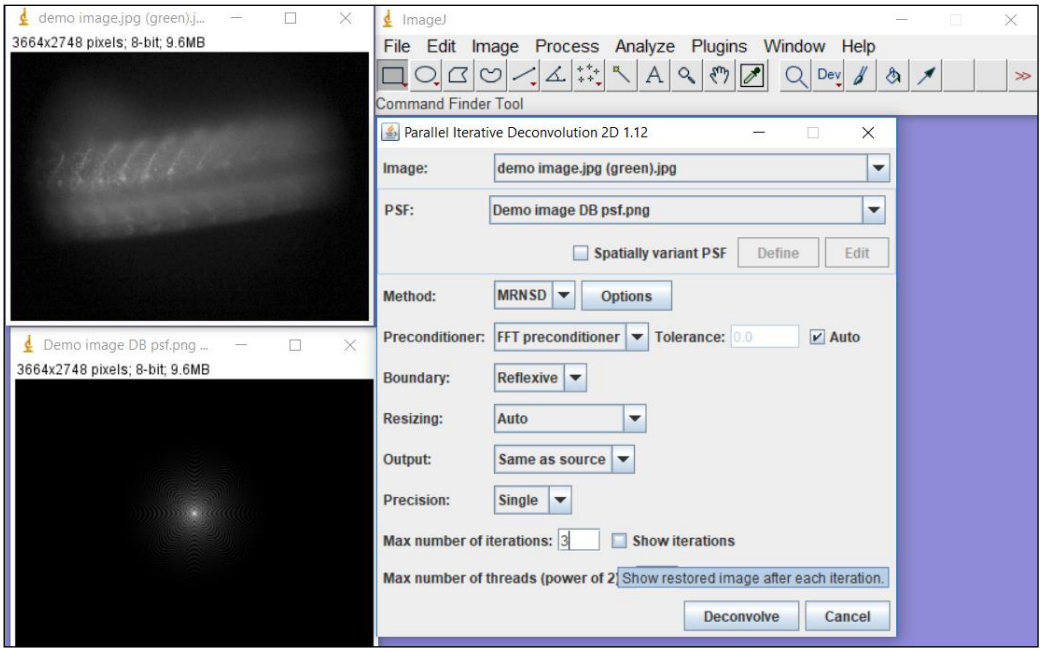

Figure 37. Various fields in PID MRNSD window

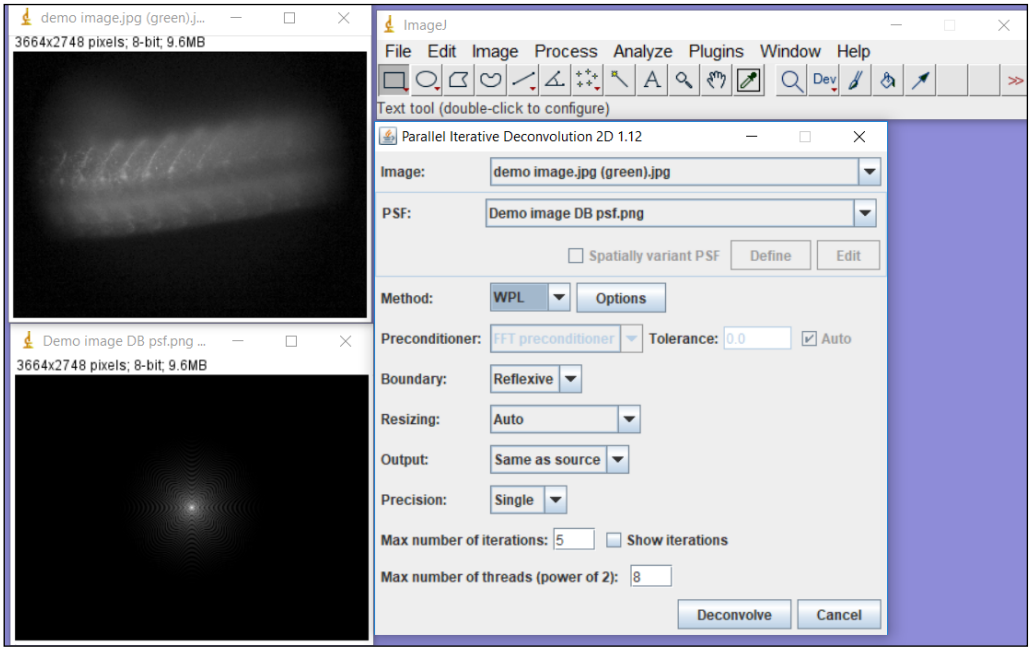

Figure 38. Various fields in PID WPL window

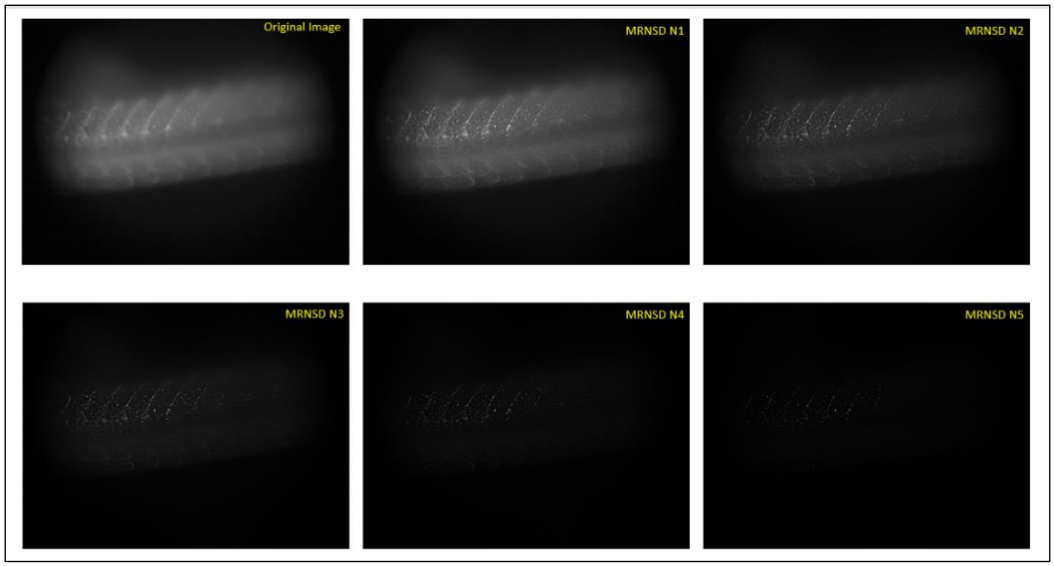

Figure 39. Resultant image after each iteration PID MRNSD algorithm

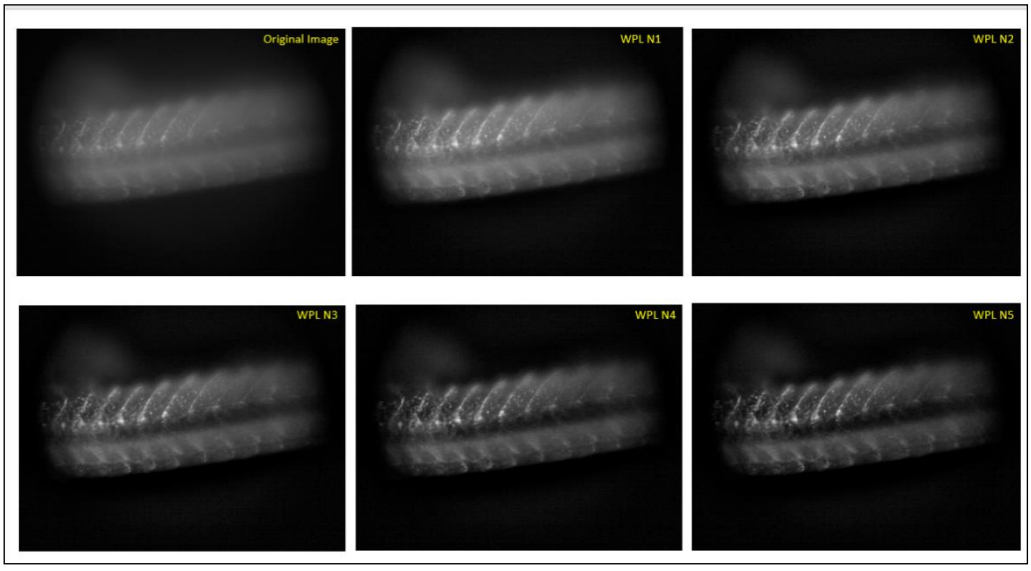

Figure 40. Resultant image after each iteration PID WPL algorithm

4.11.4.6 STEP 6 – Merge all deconvoluted singled channel images

As you can see, in the step five we deconvolute using the green channel. In same way you need to deconvolute other blue and green channels also. And merge them together later.

Note: If you have an image having only one colour florescence, then you don't have to deconvolve each channel of three i.e. red, green and blue channel image individually. For example, in our case, we are having only Green coloured florescence images so we will

deconvolute only Green channel grey scale image along with PSF image and merge it later. A demonstration is shown in figure 41-43.

There are following steps to merge channelled images

a) Go to ‘colour’ option in ‘image’ drop down menu in ImageJ software. Select merge channels (figure 41)

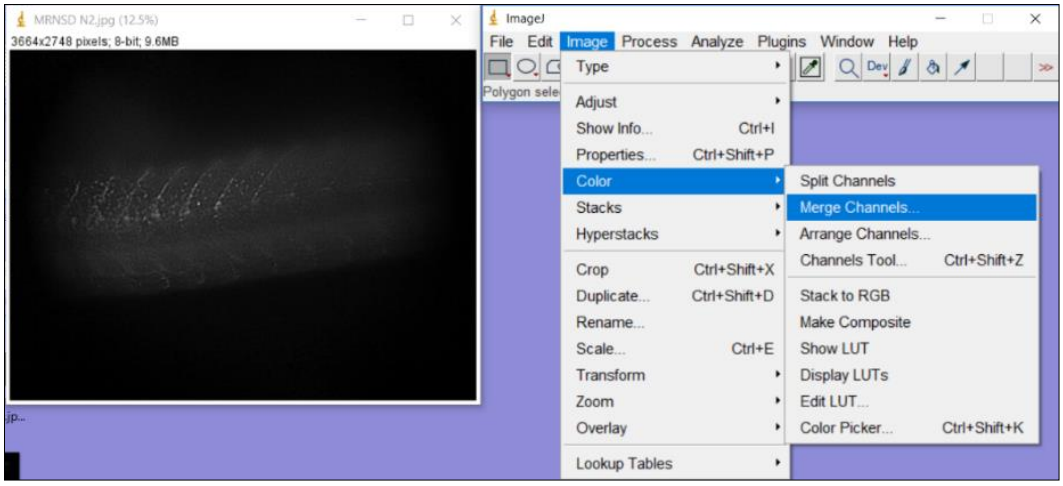

Figure 41. Merging channels

b) A new window will open containing seven channels for different colours. Choose your image in its respective channel. Uncheck the box ‘create composite’ and check the box ‘keep source images (figure 42).

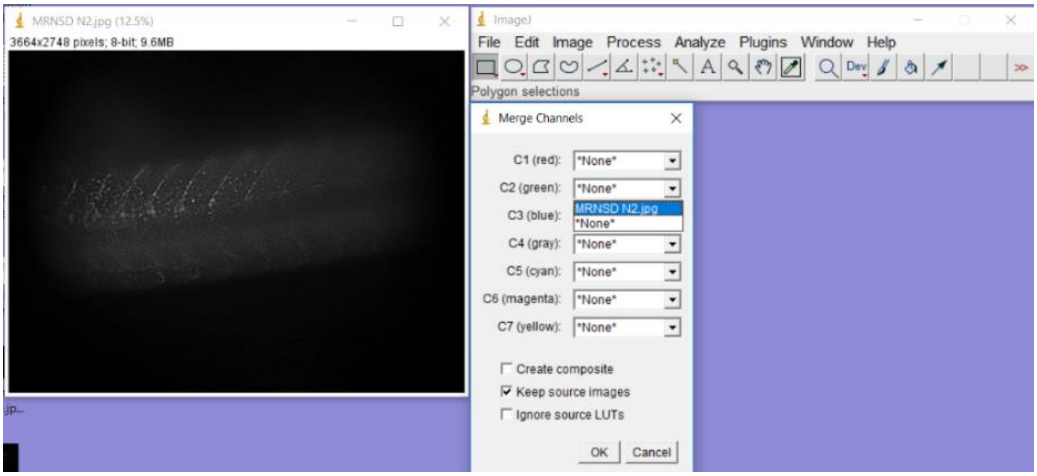

Figure 42. Selecting image in its respective channel according to colour

c) Click ok. You will get your final coloured deconvoluted image (figure 43).

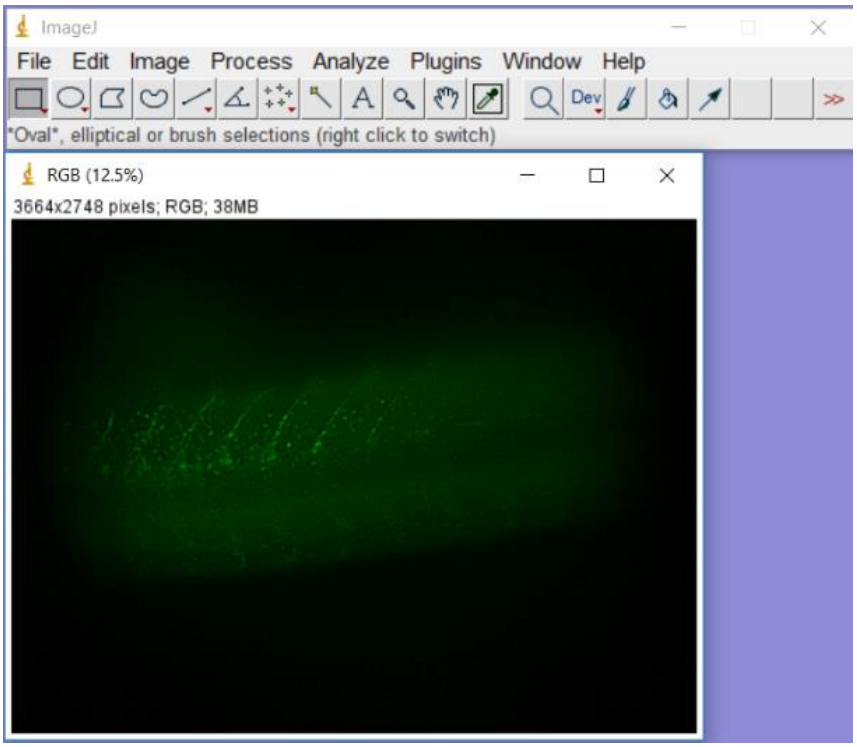

Figure 43. Shows final colouered deconvoluted image after merging channels

4.13 Statistics

For all the statistical test analysis, we used GraphPad prism software version 8.0.1. Image analysis was done with the help of Image J software. statistical analysis was performed using GraphPad Prism v8.0.1. Results are presented as mean and SEM values and statistical significance is reported as follows - (* $p \leq 0.05$, ** $p \leq 0.001$ and *** $p \leq 0.0001$)

5. Results

5.1 Combined exposure of TCS and Glyphosate is more toxic as compared to individual exposure of TCS and glyphosate

In our lab, individual toxic effects of glyphosate and TCS toxicity has already been observed. My lab members have already determined LC_{50} value of both TCS and glyphosate in their study. LC_{50} value of TCS is 0.6 µg/ml for 96 h exposure. And LC_{50} value for glyphosate is 66 ± 4.6 µg/ml for 48 h exposure and 61 ± 0.7 for glyphosate for 72 h exposure. Four concentrations were chosen to study combined exposure toxicity on zebrafish embryos viz. 50 µg/ml and 100 µg/ml for glyphosate and 0.3 µg/ml and 0.6 µg/ml for TCS were chosen.

5.1.1 Mortality rate

To observe mortality rate, chemical treatment was started using 5 hpf embryos and exposed to chemicals for 96 h. Larvae were treated with various concentration (0.3 µg/ml TCS, 0.6 µg/ml TCS, 50 µg/ml glyphosate, 100 µg/ml glyphosate, 50µg/ml glyphosate+ 0.3 TCS, 50 µg/ml glyphosate + 0.6 µg/ml TCS, 100 µg/ml glyphosate + 0.3 µg/ml TCS, 100 µg/ml glyphosate + 0.6 µg/ml TCS. Mortality was observed at end of every 24 h window and solutions were replaced with fresh ones and dead embryos were removed from solution. Finally, after 96 h exposure, percent mortality rate was calculated for each concentration.

In this study, control and solvent control showed a mean mortality rate of 2.498% and 2.666% respectively. 0.3 µg/ml and 0.6 µg/ml showed a mean mortality of 27.2% and 47.616% respectively. Combined exposure of 50G+0.3TCS (44.28%) and 50G+0.6TCS (58.732%) showed a significant increase in mean mortality rate as compared to single exposure of 50G (30.9%), 0.3TCS (27.2%) and 0.6TCS (47.616%).
However, in case of combined exposure of 100G+0.3TCS (84.816%) and 100G+0.6TCS (88.082%), we did not observe any significant change as compared to single exposure of 100G (74.032%).

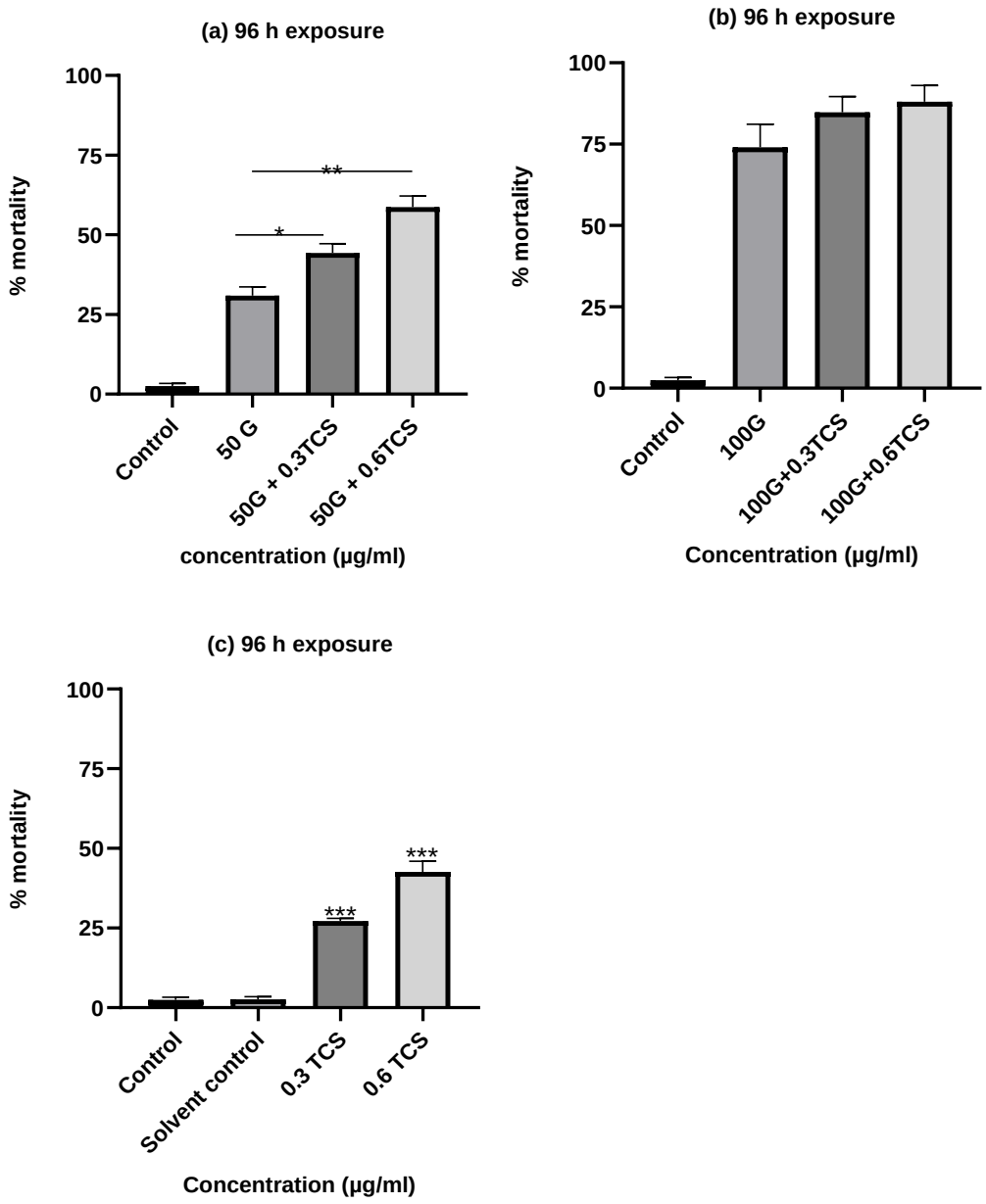

Figure 44. Mortality rate of zebrafish larva after 96 h of chemical exposure with TCS and glyphosate. (a) Combined exposure of 50G+0.3TCS (44.28%) and 50G+0.6TCS (58.732%) showed a significant increase in mean mortality rate as compared to single exposure of 50G (30.9%), 0.3TCS (27.2%) and 0.6TCS (47.616%). (b) combined exposure of 100G+0.3TCS (84.816%) and 100G+0.6TCS (88.082%), we did not observe any significant change as compared to single exposure of 100G (74.032%). (c) shows mortality rate of TCS exposure with 0.3TCS (71.06%) and 0.6TCS (50.40%). {Control(n=240), solvent control(n=240), 0.3 TCS(n=340), 0.6TCS(n=340), 50G(n=440), 100G(N=440), 50G+0.3TCS (n=440),

50G+0.6TCS (n=440), 100G+0.3TCS (n=440), 100G+0.6TCS (n=440)}. No of experiments = 5. (* $p \leq 0.05$, ** $p \leq 0.001$ and *** $p \leq 0.0001$)

5.1.2 Hatching rate

To observe hatching rate, chemical treatment was started using 5 hpf embryos and continued for 48 h. Larvae were treated with various concentration (0.3 µg/ml TCS, 0.6 µg/ml TCS, 50 µg/ml glyphosate, 100µg/ml glyphosate, 50µg/ml glyphosate+ 0.3 TCS, 50 µg/ml glyphosate + 0.6 µg/ml TCS, 100 µg/ml glyphosate + 0.3 µg/ml TCS, 100 µg/ml glyphosate + 0.6 µg/ml TCS. Solutions were replaced with fresh ones at every 24 h duration and dead embryos were removed each time. After of 48 h exposure, hatching rate was calculated for each concentration.

In our study, 0.3 µg/ml and 0.6 µg/ml of TCS exposure showed delayed hatching of 27.2% and 47.616% respectively. Combined exposure of 50G+0.6TCS (16.45%) showed a significant decrease in hatching rate as compared to single exposure of 50G (44.09%), 0.3TCS (71.06%) and 0.6TCS (50.40%).

Similar results were observed in case of combined exposure of 100G+0.3TCS (18.83%) and 100G+0.6TCS (10.18%) showed a significant decrease in mean hatching rate as compared to single exposure of 100G (29.13%), 0.3TCS (71.06%) and 0.6TCS (50.40%).

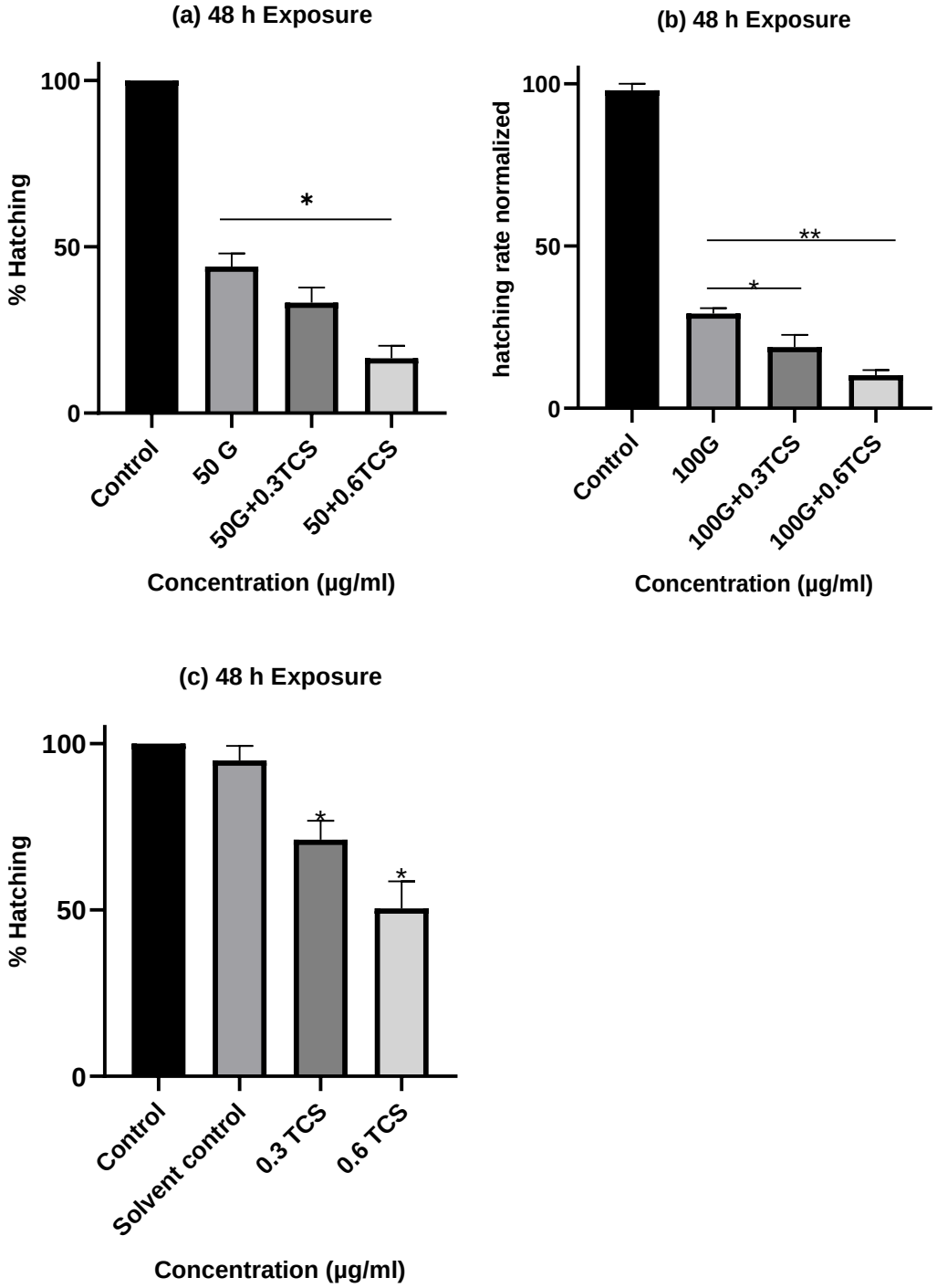

Figure 45. Hatching rate of zebrafish larva after 48 h of chemical exposure with TCS and glyphosate. (a) Combined exposure of 50G+0.6TCS (16.45%) showed a significant increase in mean hatching rate as compared to single exposure of 50G (44.09%). (b) combined exposure of 100G+0.3TCS (18.83%) and 100G+0.6TCS (10.18%) showed a significant

increase in mean mortality rate as compared to single exposure of 100G (29.13%), (c) shows mortality rate of TCS exposure with 0.3TCS (27.2%) and 0.6TCS (47.616%). {Control (n=240), solvent control (n=240), 0.3 TCS (n=340), 0.6TCS (n=340), 50G (n=440), 100G (N=440), 50G+0.3TCS (n=440), 50G+0.6TCS (n=440), 100G+0.3TCS (n=440), 100G+0.6TCS (n=440)} from 5 different experiments in all concentrations. (* $p \leq 0.05$, ** $p \leq 0.001$ and *** $p \leq 0.0001$)

5.1.3 Morphological abnormalities

To observe abnormalities in larvae, chemical treatment was started using 5 hpf embryos and continued till 72 h. Solutions were replaced with fresh ones at every 24 h duration. Larvae were treated with various concentration (0.3 µg/ml TCS, 0.6 µg/ml TCS, 50 µg/ml glyphosate, 100µg/ml glyphosate, 50µg/ml glyphosate+ 0.3 TCS, 50 µg/ml glyphosate + 0.6 µg/ml TCS, 100 µg/ml glyphosate + 0.3 µg/ml TCS, 100 µg/ml glyphosate + 0.6 µg/ml TCS. At the end of 72 h exposure, 15 larvae from each concentration were selected randomly and observed for any kind of abnormality under microscope such as yolk sac edema, tail bending, pericardial edema and spinal curvature.

In our study, 0.3 µg/ml and 0.6 µg/ml exposure did not cause any significant abnormality. 50G+0.6TCS (24.16%) displayed a significant increase in abnormality rate as compared to single exposure of 50G (11.66%) whereas 50G+0.3TCS did not show any significant difference.

Similarly, 100G+0.6TCS (10.18%) showed significant increase in abnormality as compared to single exposure of 100G (29.13%).

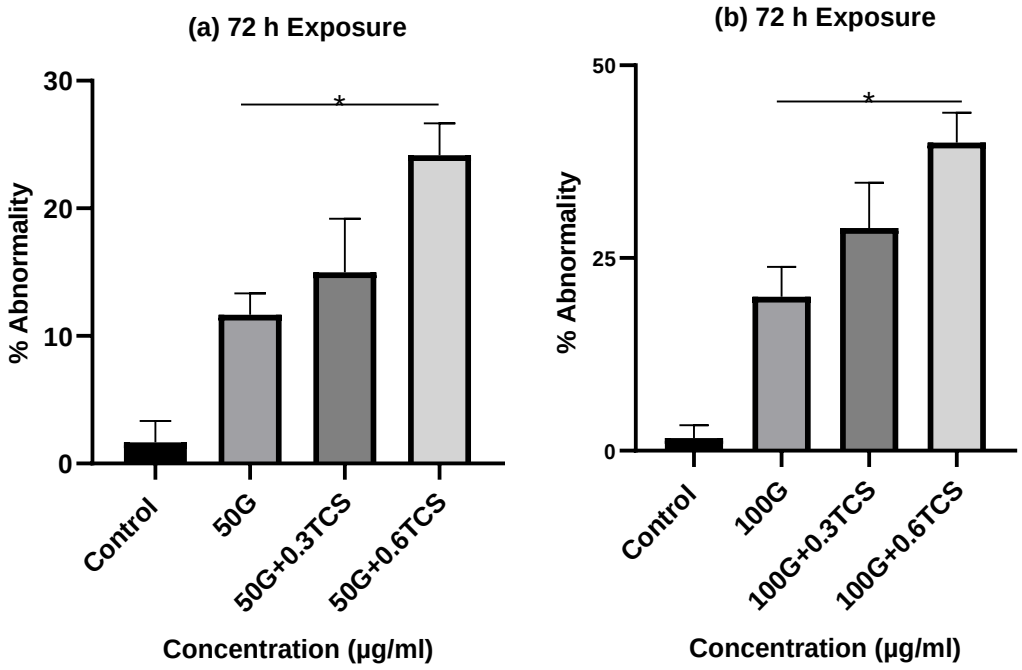

Figure 46. % abnormality of zebrafish larva after 72 h chemical exposure with TCS and glyphosate. (a) 50G+0.6TCS showed a significant increase in % abnormality as compared to 50G. (n = 15 from each experiment, no of experiments = 4) (b) combined exposure of 100G+0.6TCS (10.18%) showed a significant increase in mean mortality rate as compared to single exposure of 100G (29.13%). (n = 15 from each experiment, no of experiments = 3). (* $p \leq 0.05$, ** $p \leq 0.001$ and *** $p \leq 0.0001$)

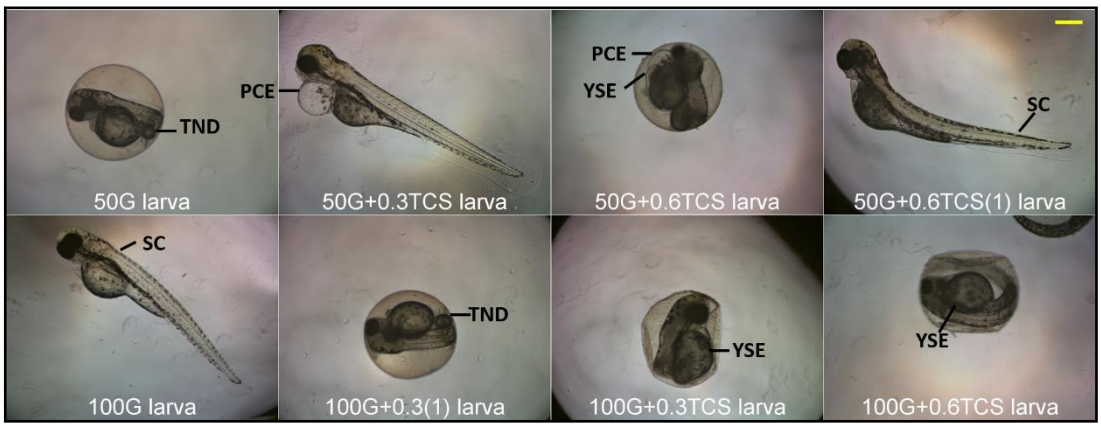

Figure 47. Pictorial representation of morphological abnormalities observed in all concentrations. TND – tail non-detachment, YSE – Yolk sac edema, SC- Spinal curvature, PCE – pericardial edema, TB – Tail bending. scale bar – 0.5 mm.

5.1.4 larval length

To study any change in larval length due to chemical exposure, chemical treatment was stated using 5 hpf embryos and continued for 96 h. Solutions were replaced with fresh solutions at every 24 h duration. Larvae were treated with various concentration (0.3 µg/ml TCS, 0.6 µg/ml TCS, 50 µg/ml glyphosate, 100µg/ml glyphosate, 50µg/ml glyphosate+ 0.3 TCS, 50 µg/ml glyphosate + 0.6 µg/ml TCS, 100 µg/ml glyphosate + 0.3 µg/ml TCS, 100 µg/ml glyphosate + 0.6 µg/ml TCS. At the end of 96 h exposure, 5 larvae from each concentration were selected randomly and their images were taken with 4x objective of Olympus X-73 microscope. Experiment was repeated four times. Length of each larva was measured with ImageJ software.

In our study, Combined exposure of 50G+0.3TCS (86.73%) and 50G+0.6TCS (84.34%) showed a significant decrease in larval length as compared to single exposure of 50G (91.04%), 0.3TCS (96.30%) and 0.6TCS (95.07%) with control length normalized (100%).

Similar results were observed in case of combined exposure of 100G+0.3TCS (83.31%) and 100G+0.6TCS (80.27%) showed a significant decrease in mean hatching rate as compared to single exposure of 100G (87.27%), 0.3TCS (96.30%) and 0.6TCS (96.07%) with control length normalized.

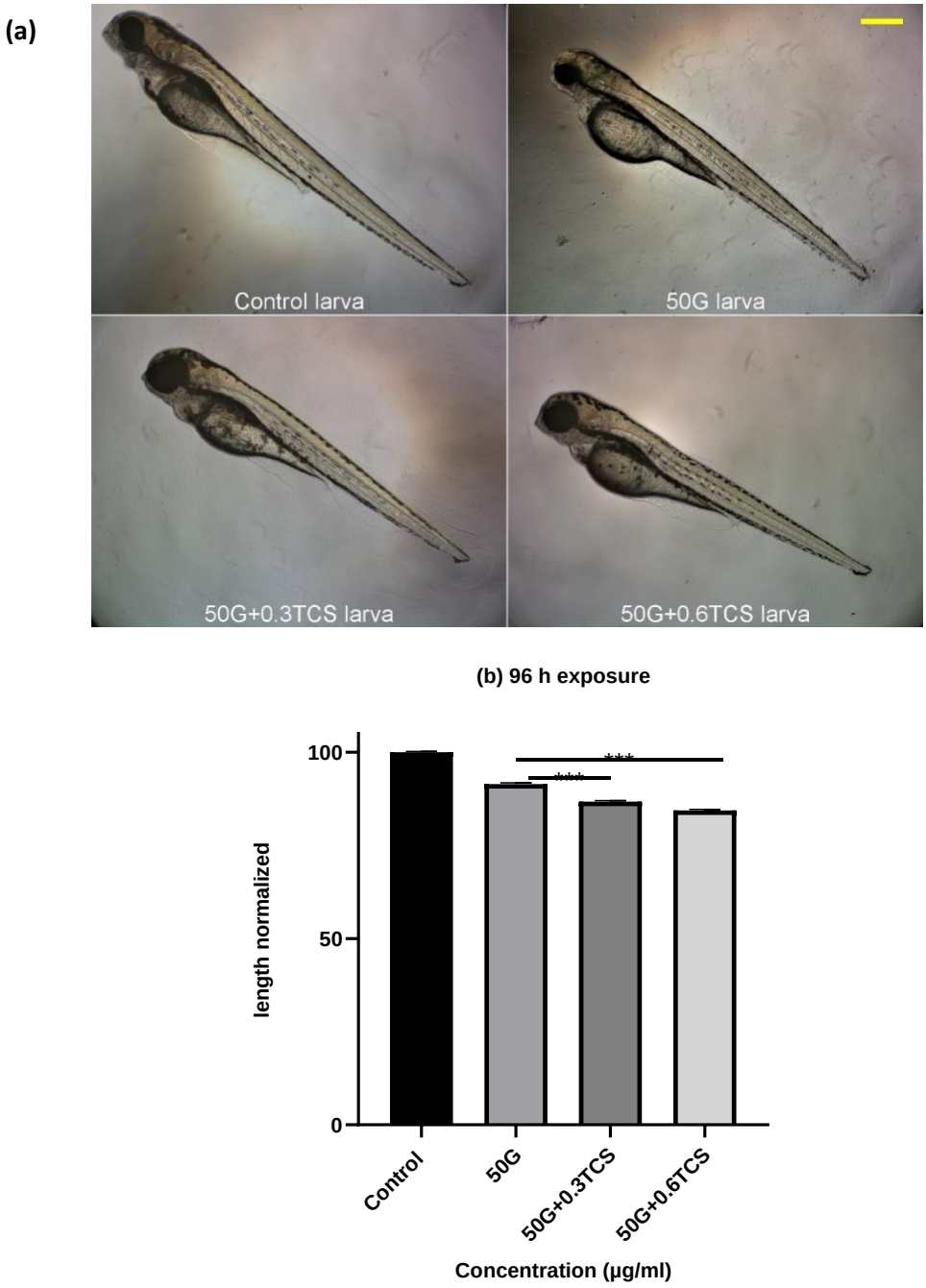

Figure 48. Larval length decreases after 96 h of combined exposure with 50G and TCS (a) Representative larval images of decreasing length along with concentration. (b) Combined exposure of 50G+0.3TCS (86.73%) and 50G+0.6TCS (84.34%) showed a significant decrease in mean larval length as compared to single exposure of 50G (91.04%). (n=5 from each experiment, no of experiments = 4). Scale bar – 0.5 mm. (* $p \leq 0.05$, ** $p \leq 0.001$ and *** $p \leq 0.0001$)

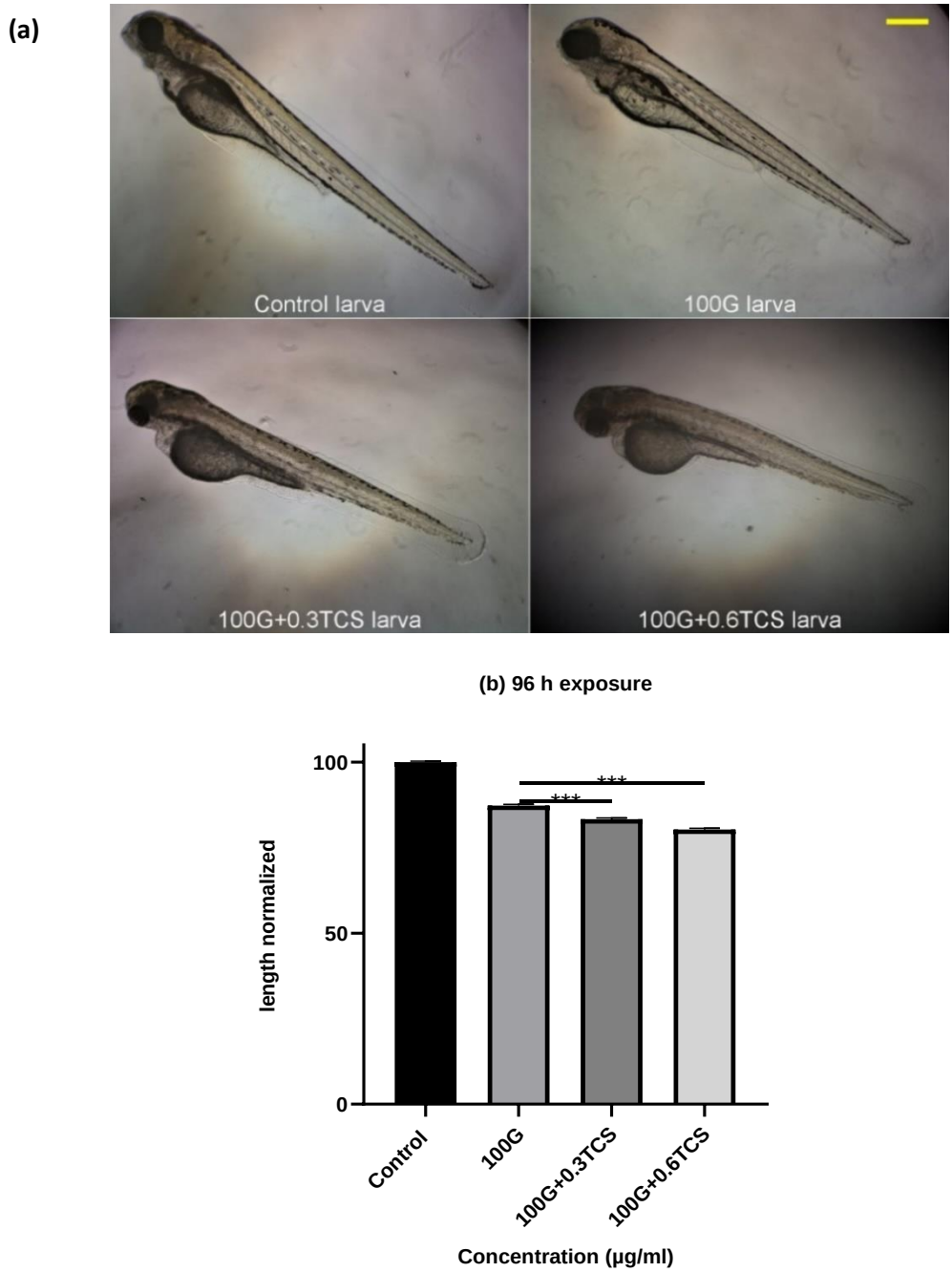

Figure 49. Larval length decreases after 96 h of combined exposure with 100G and TCS (a) Representative larval images of decreasing length along with concentration. (b) Combined exposure of 100G+0.3TCS (83.31%) and 100G+0.6TCS (80.27%) showed a significant decrease in mean larval length as compared to single exposure of 100G (87.23%). (n=5 from each experiment, no of experiments = 3). Scale bar – 0.5 mm. (* $p \leq 0.05$, ** $p \leq 0.001$ and *** $p \leq 0.0001$)

(a)

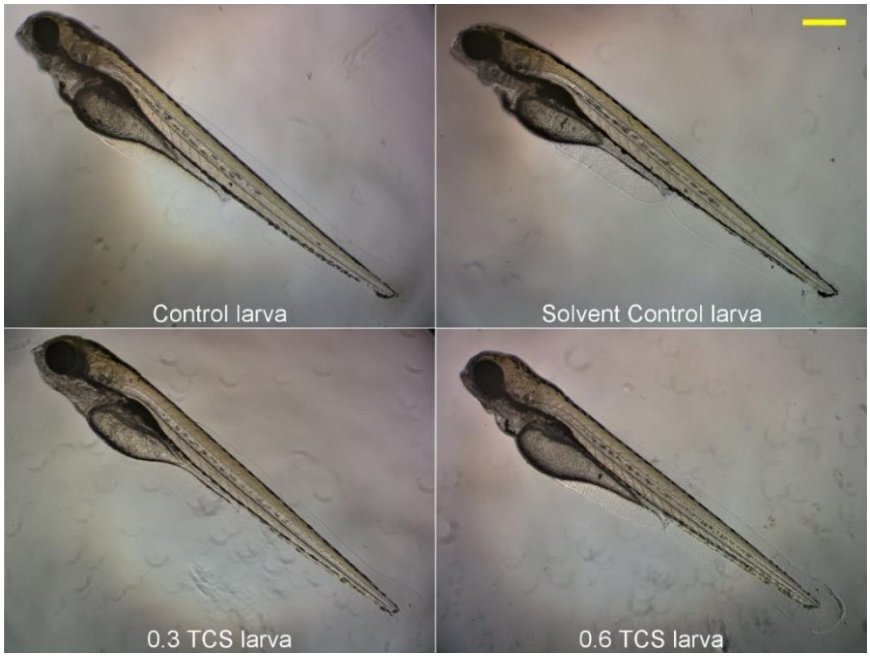

(b) 96 h exposure

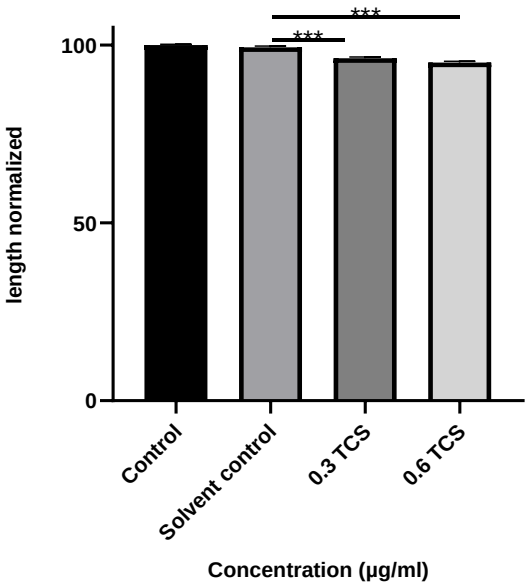

Figure 50. Larval length decreases after 96 h of chemical exposure with TCS. (a) Representative larval images of decreasing length along with concentration. (b) Chemical exposure of 0.3TCS (97.03%) and 0.6TCS (96.03%) showed a significant decrease in mean larval length as compared to control length normalized. (n=5 from each experiment, no of experiments = 4). Scale bar – 0.5 mm (*** $p \leq 0.0001$, $p \leq 0.001$ and $p \leq 0.05$

5.2 ImageJ plugin PID (WPL algorithm) delivers higher quality deconvoluted images

For deconvolution, two plugins of ImageJ PID and DLab2 were compared with each other. Then total 3 best algorithms from both plugins PID (WPL & MRNSD) and DLab2 (RL) were finally compared using a total of five sample images. Figure 51 shows the comparison between deconvolution results of both plugins using 2 sample images. Both algorithms of PID provided better result in each sample image.

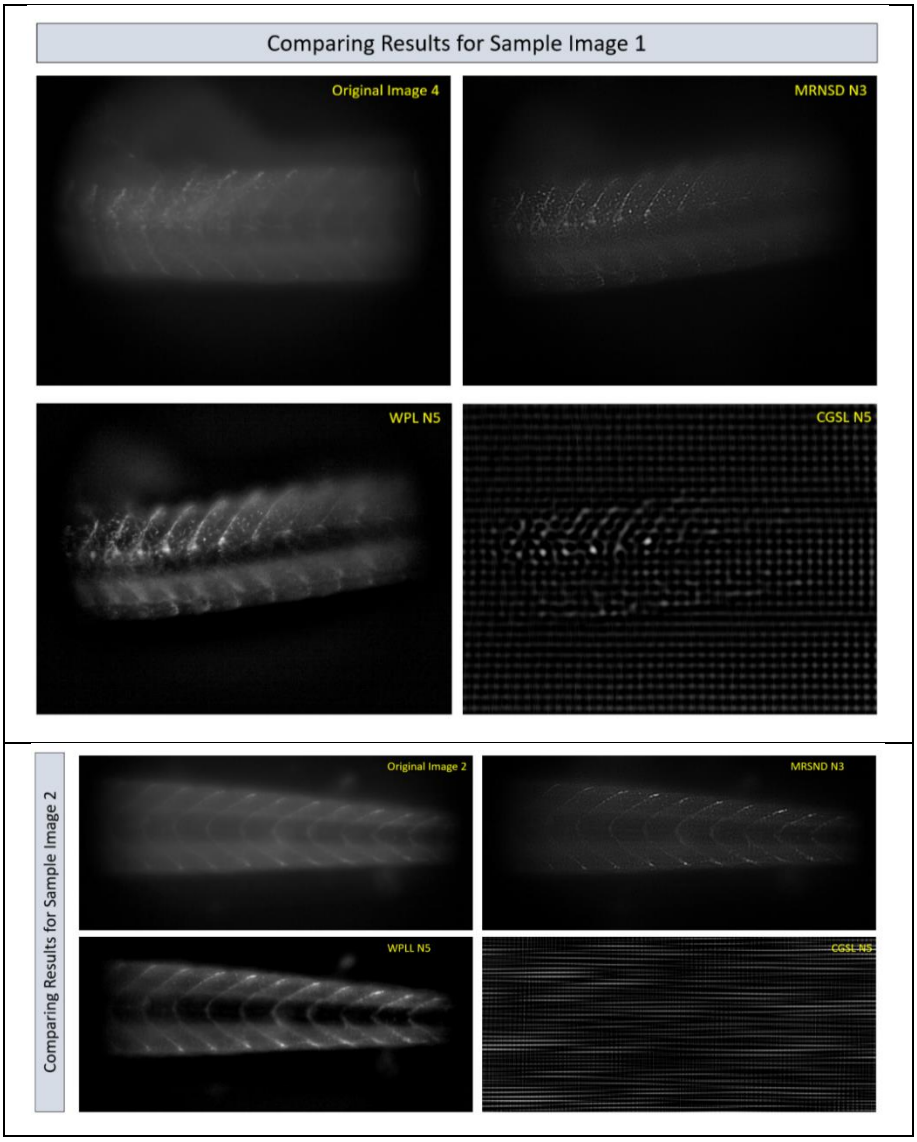

Figure 51. Comparison Between PID and Dlab2 plugin deconvolution

Then both algorithms of PID were compared with each other using five sample images. Since PID allows us to analyse resultant image after each iteration, figures 52-53 compare

both WPL and MRNSD algorithms of PID showing 5 resultant images obtained after each iteration.

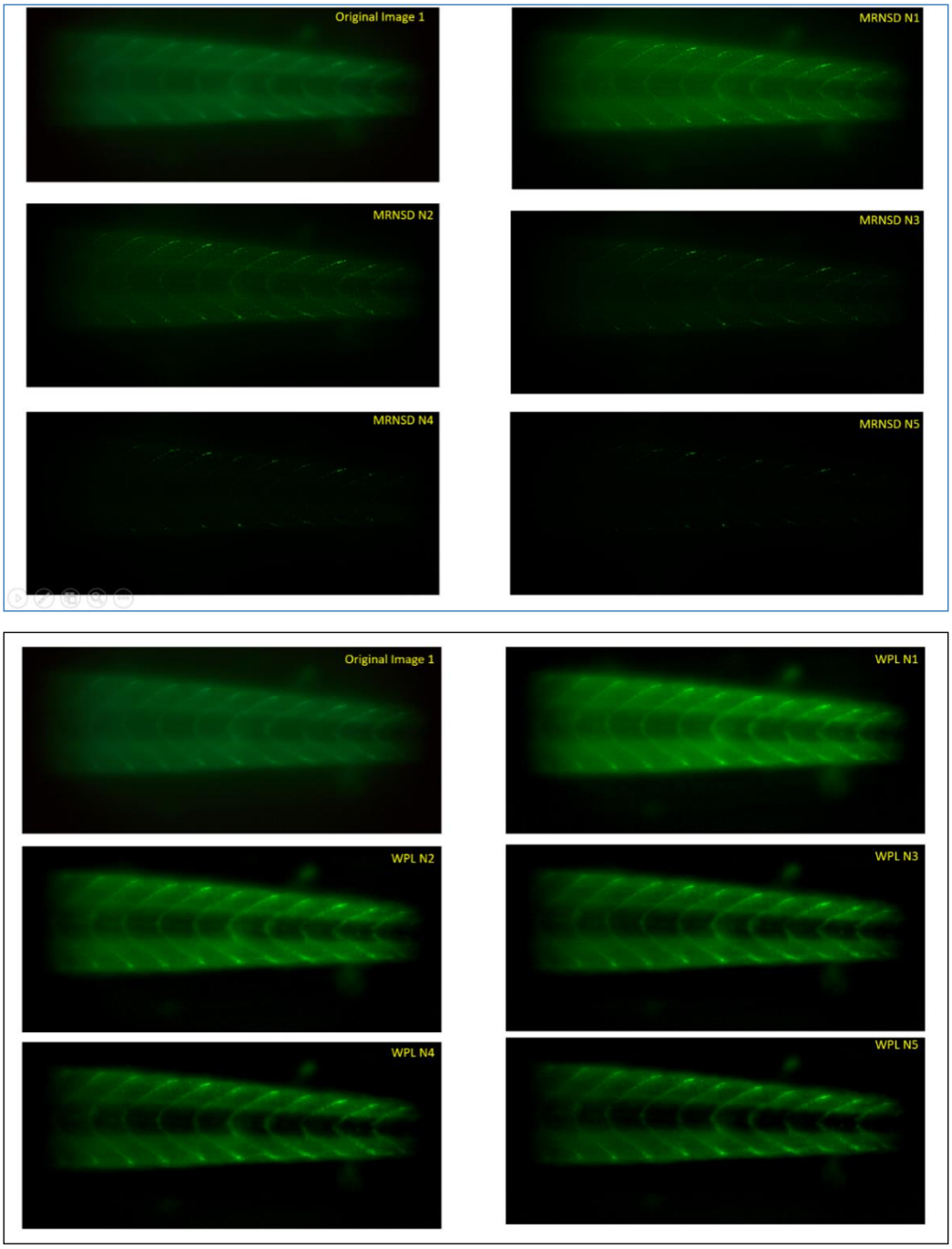

Figure 52.. Comparison each iteration using PID MRNSD and PID WPL

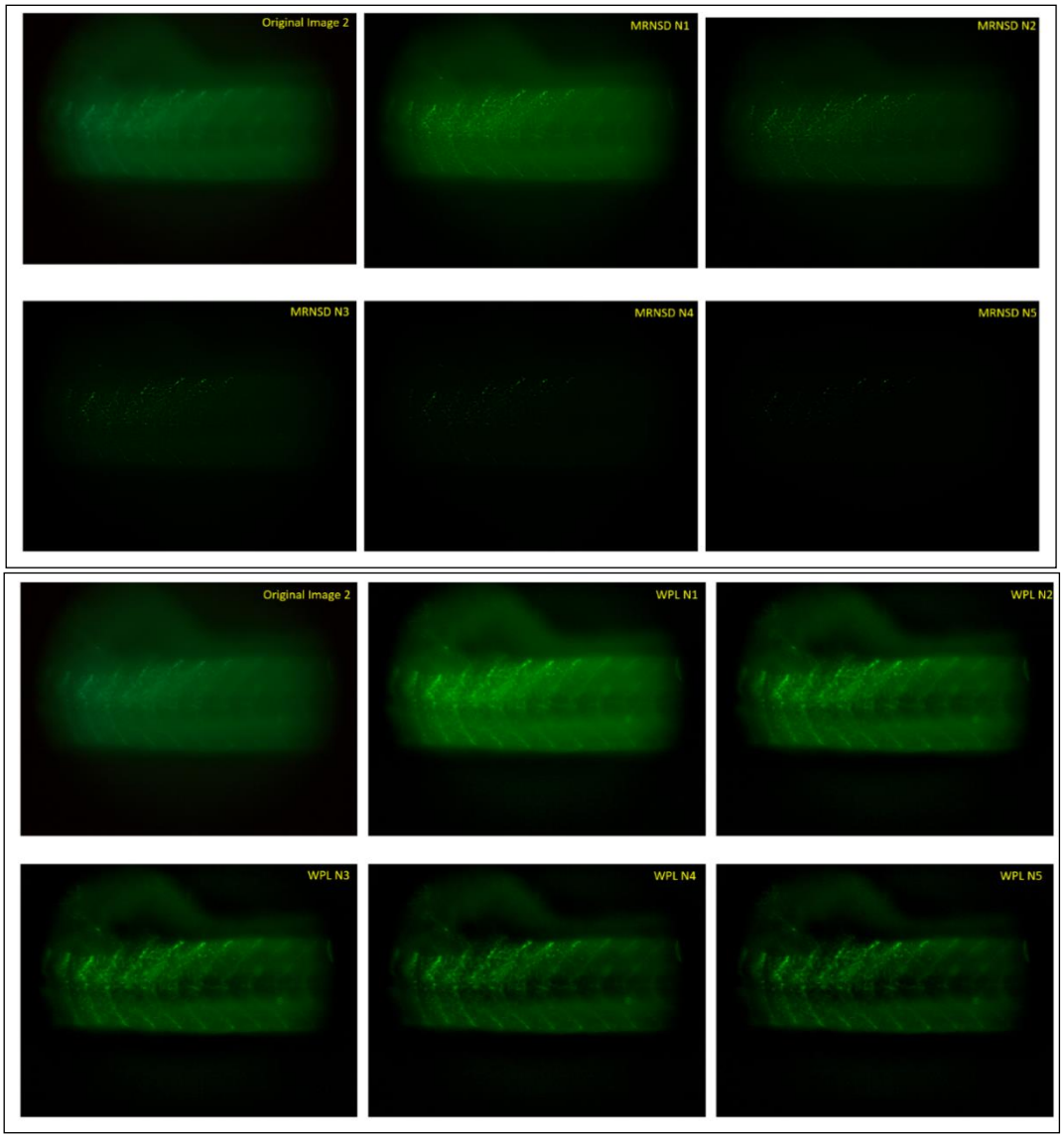

Figure 53.. Comparison of iterations using PID MRNSD and PID WPL

5.3 TCS affects NMJ integrity

5.3.1 TCS induced Change in chevron angle

To analyse chevron angle, a definite region comprised of a total of 5 segments above the middle trunk of larvae was chosen for analytical purposes as shown in figure 10. A total of 15-17 larvae from 4 individual experiments {Control (n=15); 0.3 µg/ml TCS treated (n = 15) and 0.6 µg/ml TCS treated (n = 17)} were analysed using ImageJ and statistical analysis was done by Mann-Witney t-test using GraphPad Prism v 8.0.1. (* $p \leq 0.05$, ** $p \leq 0.001$ and *** $p \leq 0.0001$)

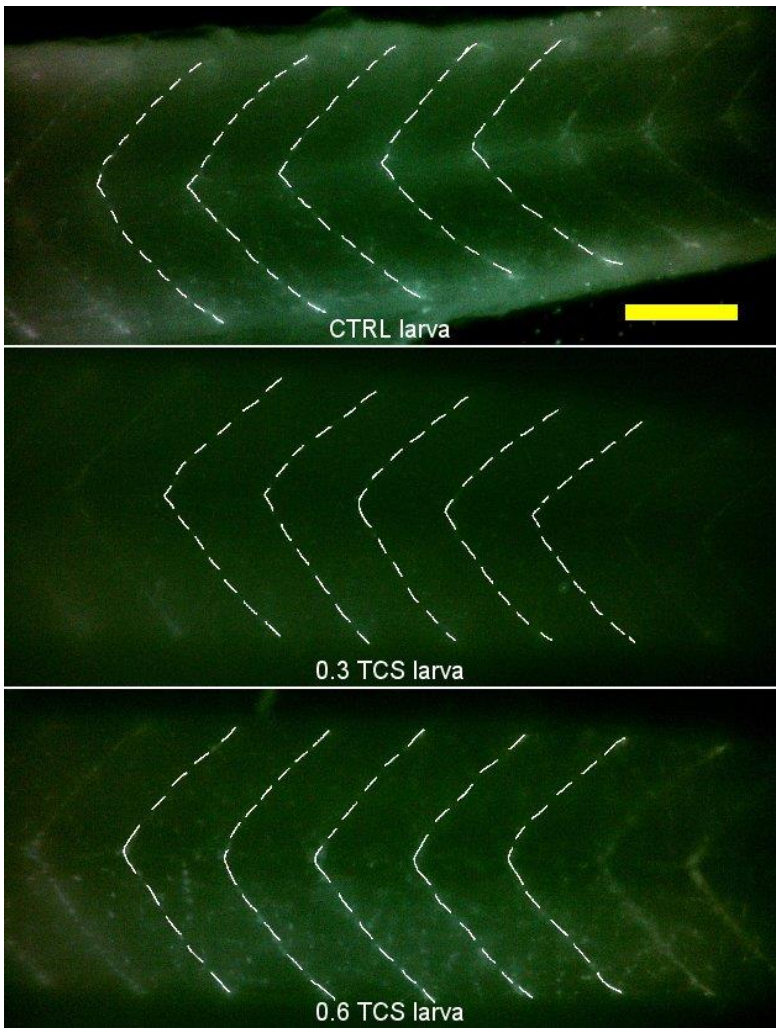

Figure 54. Representative images showing an increase in chevron angle in TCS exposed larva

Figure 54 shows pictorial presentation of chevron angle change induced due to TCS treatment in zebrafish larva. Control (n=15); 0.3 µg/ml TCS treated (n = 15) and 0.6 µg/ml TCS treated (n = 17) larvae were analysed. 0.3 TCS and 0.6 TCS refers to 0.3 µg/ml and 0.6 µg/ml TCS concentration treated larvae. TCS seems to cause concentration dependent increase in chevron angle. Scale bar – 0.5 mm.

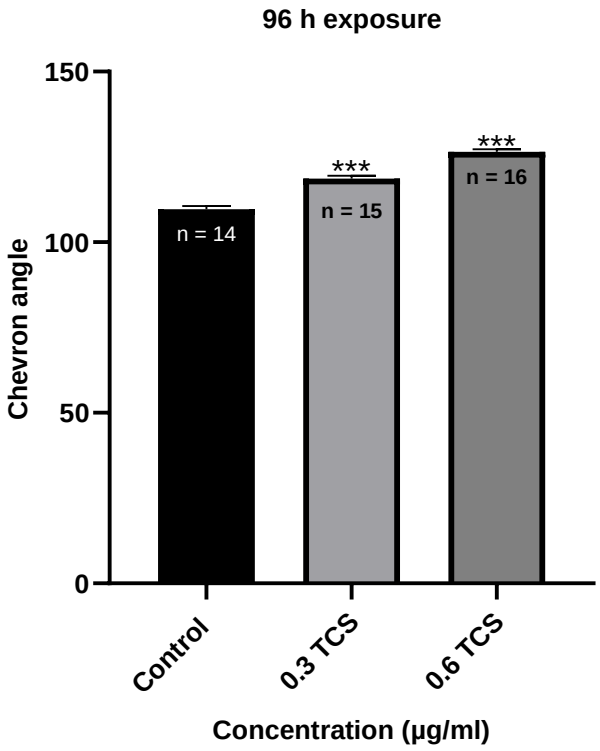

Figure 55. Graph representing TCS induced chevron angle change.

Figure 55. shows graphical presentation of chevron angle change induced due to TCS treatment in zebrafish larva. Graph was plotted by taking TCS concentration on x-axis and chevron angle on y-axis. We observed that TCS causes concentration-dependent increase in chevron angle. 0.3 and 0.6 TCS refers to 0.3 µg/ml and 0.6 µg/ml TCS concentration treated larvae while '0' represents chevron angle of control larva. We observed that control larvae showed a mean chevron angle of 109.65˚ whereas 0.3 µg/ml and 0.6 µg/ml TCS treated larvae showed mean chevron angle of 118.68˚and 126.46˚respectively. (* $p \leq 0.05$, ** $p \leq 0.001$ and *** $p \leq 0.0001$)

5.3.2 TCS induced NMJ irregularities

To analyse NMJ discontinuities, A definite region comprised of a total of 11 segments above the middle trunk of larvae was chosen for analytical purposes as shown in figure 10. A total of 9-11 larvae from 3 individual experiments [Control (n=9); 0.3 µg/ml TCS treated (n = 9) and 0.6 µg/ml TCS treated (n = 11)] were analysed using ImageJ and statistical analysis was done by unpaired t-test using GraphPad Prism v 8.0.1.(* $p \leq 0.05$, ** $p \leq 0.001$ and *** $p \leq 0.0001$).

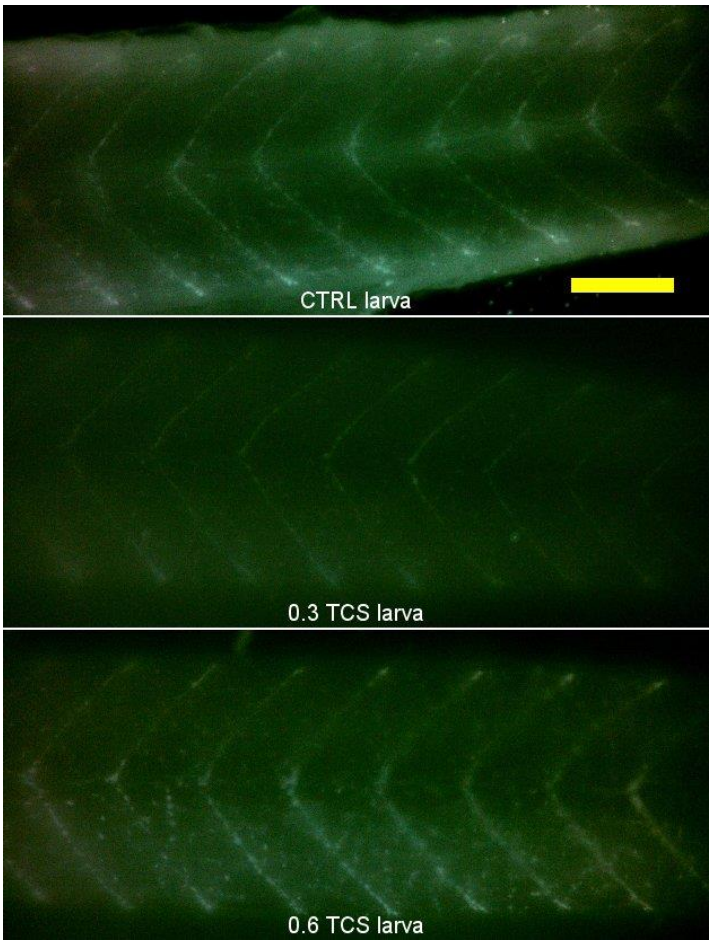

Figure 56. Representative images of the zebrafish larvae showing discontinuities in NMJ

Figure 56. Pictorial presentation of NMJ irregularities in control as well as treated larvae. A total of 9-11 larvae {Control (n=9); 0.3 µg/ml TCS treated (n = 9) and 0.6 µg/ml TCS treated (n = 11)} larvae were analysed. 0.3 TCS and 0.6 TCS refers to 0.3 µg/ml and 0.6

µg/ml TCS concentration treated larvae. TCS seems to cause concentration dependent increase in chevron angle. Scale bar – 0.5 mm

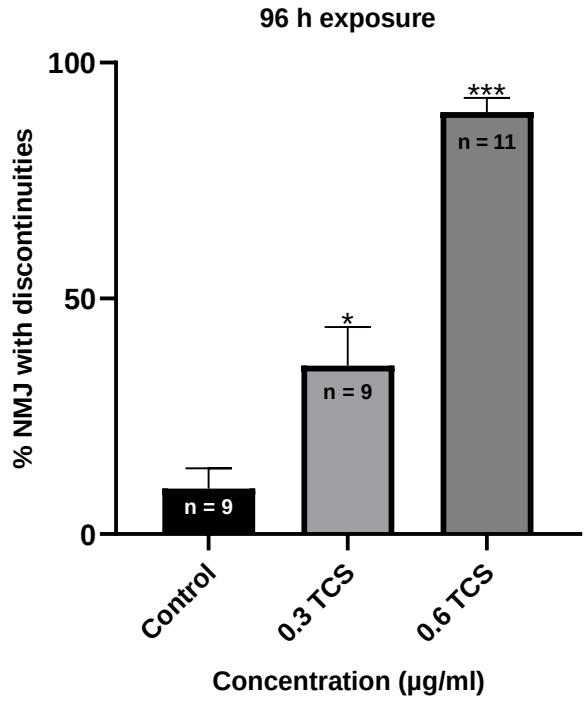

Figure 57. Graph representing TCS induced NMJ discontinuities

Figure 57. shows graphical presentation of NMJ irregularities induced due to TCS treatment in zebrafish larva. Graph was plotted by taking TCS concentration and % no of segments on the x-axis and y-axis respectively. We observed that TCS causes concentration-dependent increase in NMJ irregularities. 0.3 and 0.6 TCS refers to 0.3 µg/ml and 0.6 µg/ml TCS concentration treated larvae while '0' represents control larva. In our study, less than 20% of segments of control larvae showed NMJ discontinuities whereas in case of 0.3 µg/ml and 0.6 µg/ml TCS treated larvae both more than 30% and 60% segments showed NMJ irregularities respectively. (* $p \leq 0.05$, ** $p \leq 0.001$ and *** $p \leq 0.0001$)

Discussion and Conclusion

In our day to day life, directly or indirectly, we are exposed to various chemicals in different concentrations. Therefore, it is the need of the hour to study the toxic effects of various chemicals individually as well as in combination with other chemicals. When an individual is exposed to two or more chemicals, they may either have agonistic or anti-agonistic effect on the individual. TCS and glyphosate are two common chemicals that have emerged as pollutants. In this project, the effects of TCS and Glyphosate have been observed on zebrafish embryos when the embryos were exposed to the above said chemicals individually or in combination.

Combined exposure of both 50G+0.3TCS and 50+0.6TCS displayed a significant increase in mortality rate as compared to single exposure of 50G. we have compared directly to 50 g here in every case because 50 G is far more toxic than TCS. However, 100G and its dual concentration, did not show any significant difference. This might be because, 100G concentration is already results in too mortal for embryos to show any significant difference with TCS concentration when combined.

Higher concentration of TCS viz. 0.6 µg/ml with both concentration of glyphosate (50 µg/ml and 100µg/ml showed significant delay in hatching rate. Similar effects were observed when comparison of abnormality occurrence was done in individual v/s combined exposure.

However, in case of larval length, a concentration-dependent decrease in length was observed. And combined exposure resulted in shorter length than single exposure in each case.

In this study, it was found that TCS is toxic at neuronal as well as muscular level. We found out that TCS dysregulates structures of both chevron angle as well as NMJ in zebrafish embryo in a concentration dependent manner. In our study, less than 20% of segments of control larvae showed NMJ discontinuities whereas in case of 0.3 µg/ml and 0.6 µg/ml TCS treated larvae more than 30% and 60% segments showed NMJ irregularities respectively. Also, control larvae showed a mean chevron angle of 109.68˚whereas 0.3 µg/ml and 0.6 µg/ml TCS treated larvae showed mean chevron angle of 118.65˚ and 126.46˚respectively.

Chevron angle of myotome is related to swimming behaviour of larva. Any change would have direct effect on swimming activity or other motor behaviour. NMJ refers to direct physical contact between nervous and muscle tissue and is responsible for neuron-derived motor behaviour of larva.

Future directions:

Our results indicate developmental toxicity upon combined exposure to TCS and glyphosate. To further evaluate the extent of neurotoxicity caused by TCS and its combined effect with glyphosate, touch evoke escape response (TEER) is used to analyse muscle performance and behavioural analysis of larva.

As already discussed before, whole mount labelling of 4-dpf larva with *Znp1* and Alexa-488 helps to analyse neuromuscular properties (NMJ) of zebrafish larva which would help deeper understanding of muscular defects (if present) in case of combined exposure.

References

Adolfsson-Erici, Margaretha, Maria Pettersson, Jari Parkkonen, and Joachim Sturve. 2002. "Triclosan, a Commonly Used Bactericide Found in Human Milk and in the Aquatic Environment in Sweden." *Chemosphere* 46(9–10):1485–89.

Agostini, Lidiane P., Raquel S. Dettogni, Raquel S. Dos Reis, Elaine Stur, Eldamária V. W. Dos Santos, Diego P. Ventorim, Fernanda M. Garcia, Rodolfo C. Cardoso, Jones B. Graceli, and Iúri D. Louro. 2020. "Effects of Glyphosate Exposure on Human Health: Insights from Epidemiological and in Vitro Studies." *The Science of the Total Environment* 705:135808.

Ait Bali, Yassine, Saadia Ba-Mhamed, and Mohamed Bennis. 2017. "Behavioral and Immunohistochemical Study of the Effects of Subchronic and Chronic Exposure to Glyphosate in Mice." *Frontiers in Behavioral Neuroscience* 11.

Ajao, Charmaine, Maria A. Andersson, Vera V. Teplova, Szabolcs Nagy, Carl G. Gahmberg, Leif C. Andersson, Maria Hautaniemi, Balazs Kakasi, Merja Roivainen, and Mirja Salkinoja-Salonen. 2015. "Mitochondrial Toxicity of Triclosan on Mammalian Cells." *Toxicology Reports* 2:624–37.

Bai, Shahla Hosseini, and Steven M. Ogbourne. 2016. "Glyphosate: Environmental Contamination, Toxicity and Potential Risks to Human Health via Food Contamination." *Environmental Science and Pollution Research International* 23(19):18988–1.

Barrett, Ruth, Clare Chappell, Marie Quick, and Angeleen Fleming. 2006. "A Rapid, High Content,in Vivo Model of Glucocorticoid-Induced Osteoporosis." *Biotechnology Journal* 1(6):651–55.

Benachour, Nora, and Gilles-Eric Séralini. 2009. "Glyphosate Formulations Induce Apoptosis and Necrosis in Human Umbilical, Embryonic, and Placental Cells." *Chemical Research in Toxicology* 22(1):97–105.

Benbrook, Charles M. 2016. "Trends in Glyphosate Herbicide Use in the United States and Globally." *Environmental Sciences Europe* 28(1).

Bento, Célia P. M., Xiaomei Yang, Gerrit Gort, Sha Xue, Ruud van Dam, Paul Zomer, Hans G. J. Mol, Coen J. Ritsema, and Violette Geissen. 2016. "Persistence of Glyphosate and Aminomethylphosphonic Acid in Loess Soil under Different Combinations of Temperature, Soil Moisture and Light/Darkness." *The Science of the Total Environment* 572:301–11.

Blagden, Chris S., Peter D. Currie, Philip W. Ingham, and Simon M. Hughes. 1997. "Notochord Induction of Zebrafish Slow Muscle Mediated by Sonic Hedgehog." *Genes & Development* 11(17):2163–75.

Borggaard, Ole K., and Anne Louise Gimsing. 2008. “Fate of Glyphosate in Soil and the Possibility of Leaching to Ground and Surface Waters: A Review.” *Pest Management Science* 64(4):441–56.

Boyce, John M., Didier Pittet, Healthcare Infection Control Practices Advisory Committee, and HICPAC/SHEA/APIC/IDSA Hand Hygiene Task Force. 2002. “Guideline for Hand Hygiene in Health-Care Settings. Recommendations of the Healthcare Infection Control Practices Advisory Committee and the HICPAC/SHEA/APIC/IDSA Hand Hygiene Task Force. Society for Healthcare Epidemiology of America/Association for Professionals in Infection Control/Infectious Diseases Society of America.” *MMWR. Recommendations and Reports: Morbidity and Mortality Weekly Report. Recommendations and Reports* 51(RR-16):1–45, quiz CE1-4.

Cai, Shaofang, Jiahao Zhu, Lingling Sun, Chunhong Fan, Yaohong Zhong, Qing Shen, and Yingjun Li. 2019. “Association Between Urinary Triclosan With Bone Mass Density and Osteoporosis in US Adult Women, 2005–2010.” *The Journal of Clinical Endocrinology and Metabolism* 104(10):4531–38.

Calafat, Antonia M., Xiaoyun Ye, Lee-Yang Wong, John A. Reidy, and Larry L. Needham. 2008. “Urinary Concentrations of Triclosan in the U.S. Population: 2003-2004.” *Environmental Health Perspectives* 116(3):303–7.

Carpenter, Joanna K., Joanne M. Monks, and Nicola Nelson. 2016. “The Effect of Two Glyphosate Formulations on a Small, Diurnal Lizard (Oligosoma Polychroma).” *Ecotoxicology (London, England)* 25(3):548–54.

Chaudhari, Umesh, Harshal Nemade, Poornima Sureshkumar, Mathieu Vinken, Gamze Ates, Vera Rogiers, Jürgen Hescheler, Jan Georg Hengstler, and Agapios Sachinidis. 2018. “Functional Cardiotoxicity Assessment of Cosmetic Compounds Using Human-Induced Pluripotent Stem Cell-Derived Cardiomyocytes.” *Archives of Toxicology* 92(1):371–81.

Chu, Shaogang, and Chris D. Metcalfe. 2007. “Simultaneous Determination of Triclocarban and Triclosan in Municipal Biosolids by Liquid Chromatography Tandem Mass Spectrometry.” *Journal of Chromatography. A* 1164(1–2):212–18.

Chuanchuen, R., K. Beinlich, T. T. Hoang, A. Becher, R. R. Karkhoff-Schweizer, and H. P. Schweizer. 2001. “Cross-Resistance between Triclosan and Antibiotics in Pseudomonas Aeruginosa Is Mediated by Multidrug Efflux Pumps: Exposure of a Susceptible Mutant Strain to Triclosan Selects NfxB Mutants Overexpressing MexCD-OprJ.” *Antimicrobial Agents and Chemotherapy* 45(2):428–32.

Cole, Nicholas J., Thomas E. Hall, Emily K. Don, Silke Berger, Catherine A. Boisvert, Christine Neyt, Rolf Ericsson, Jean Joss, David B. Gurevich, and Peter D. Currie. 2011. “Development and Evolution of the Muscles of the Pelvic Fin.” *PLoS Biology* 9(10):e1001168.

Devoto, S. H., E. Melançon, J. S. Eisen, and M. Westerfield. 1996. “Identification of Separate Slow and Fast Muscle Precursor Cells in Vivo, Prior to Somite Formation.” *Development (Cambridge, England)* 122(11):3371–80.

Devoto, S. H., W. Stoiber, C. L. Hammond, P. Steinbacher, J. R. Haslett, M. J. F. Barresi, S. E. Patterson, E. G. Adiarte, and S. M. Hughes. 2006. “Generality of Vertebrate Developmental Patterns: Evidence for a Dermomyotome in Fish.” *Evolution & Development* 8(1):101–10.

Dhillon, Gurpreet Singh, Surinder Kaur, Rama Pulicharla, Satinder Kaur Brar, Maximiliano Cledón, Mausam Verma, and Rao Y. Surampalli. 2015. “Triclosan: Current Status, Occurrence, Environmental Risks and Bioaccumulation Potential.” *International Journal of Environmental Research and Public Health* 12(5):5657–84.

Du, S. J., S. H. Devoto, M. Westerfield, and R. T. Moon. 1997. “Positive and Negative Regulation of Muscle Cell Identity by Members of the Hedgehog and TGF-Beta Gene Families.” *The Journal of Cell Biology* 139(1):145–56.

Duke, Stephen O. 2018. “The History and Current Status of Glyphosate.” *Pest Management Science* 74(5):1027–34.

Falisse, Elodie, Anne-Sophie Voisin, and Frédéric Silvestre. 2017. “Impacts of Triclosan Exposure on Zebrafish Early-Life Stage: Toxicity and Acclimation Mechanisms.” *Aquatic Toxicology (Amsterdam, Netherlands)* 189:97–107.

Fiss, E. Matthew, Krista L. Rule, and Peter J. Vikesland. 2007. “Formation of Chloroform and Other Chlorinated Byproducts by Chlorination of Triclosan-Containing Antibacterial Products.” *Environmental Science & Technology* 41(7):2387–94.

Fluegge, Keith R., and Kyle R. Fluegge. 2015. “Glyphosate Use Predicts ADHD Hospital Discharges in the Healthcare Cost and Utilization Project Net (HCUPnet): A Two-Way Fixed-Effects Analysis.” *PLoS ONE* 10(8).

Fortes, Cristina, Simona Mastroeni, Marjorie Segatto M, Clarissa Hohmann, Lucia Miligi, Lucio Bakos, and Renan Bonamigo. 2016. “Occupational Exposure to Pesticides With Occupational Sun Exposure Increases the Risk for Cutaneous Melanoma.” *Journal of Occupational and Environmental Medicine* 58(4):370–75.

Fox, Michael A., and Joshua R. Sanes. 2007. “Synaptotagmin I and II Are Present in Distinct Subsets of Central Synapses.” *The Journal of Comparative Neurology* 503(2):280–96.

Gaur, Himanshu, and Anamika Bhargava. 2019. “Glyphosate Induces Toxicity and Modulates Calcium and NO Signaling in Zebrafish Embryos.” *Biochemical and Biophysical Research Communications* 513(4):1070–75.

Gee, R. H., A. Charles, N. Taylor, and P. D. Darbre. 2008. “Oestrogenic and Androgenic Activity of Triclosan in Breast Cancer Cells.” *Journal of Applied Toxicology: JAT* 28(1):78–91.

George, Jasmine, and Yogeshwer Shukla. 2013. “Emptying of Intracellular Calcium Pool and Oxidative Stress Imbalance Are Associated with the Glyphosate-Induced Proliferation in Human Skin Keratinocytes HaCaT Cells.” *ISRN Dermatology* 2013:825180.

Giannini, Asa, and John Giannini. n.d. “2D and 3D Fluorescence Deconvolution Manual.” 32.

Gimsing, A. L., O. K. Borggaard, and M. Bang. 2004. “Influence of Soil Composition on Adsorption of Glyphosate and Phosphate by Contrasting Danish Surface Soils.” *European Journal of Soil Science* 55(1):183–91.

Halpern, Marnie E., Robert K. Ho, Charline Walker, and Charles B. Kimmel. 1993. “Induction of Muscle Pioneers and Floor Plate Is Distinguished by the Zebrafish No Tail Mutation.” *Cell* 75(1):99–111.

Heath, Richard J., Jing Li, Gregory E. Roland, and Charles O. Rock. 2000. “Inhibition of the Staphylococcus AureusNADPH-Dependent Enoyl-Acyl Carrier Protein Reductase by Triclosan and Hexachlorophene.” *Journal of Biological Chemistry* 275(7):4654–59.

Hoang, T. T., and H. P. Schweizer. 1999. “Characterization of Pseudomonas Aeruginosa Enoyl-Acyl Carrier Protein Reductase (FabI): A Target for the Antimicrobial Triclosan and Its Role in Acylated Homoserine Lactone Synthesis.” *Journal of Bacteriology* 181(17):5489–97.

JAMES, Margaret O., Christopher J. MARTH, and Laura ROWLAND-FAUX. 2012. “Slow O-Demethylation of Methyl Triclosan to Triclosan, Which Is Rapidly Glucuronidated and Sulfonated in Channel Catfish Liver and Intestine.” *Slow O-Demethylation of Methyl Triclosan to Triclosan, Which Is Rapidly Glucuronidated and Sulfonated in Channel Catfish Liver and Intestine* 124–25:72–82.

Kim, Jin, Hanseul Oh, Bokyeong Ryu, Ukjin Kim, Ji Min Lee, Cho-Rok Jung, C. Yoon Kim, and Jae-Hak Park. 2018. “Triclosan Affects Axon Formation in the Neural Development Stages of Zebrafish Embryos (Danio Rerio).” *Environmental Pollution (Barking, Essex: 1987)* 236:304–12.

Kimmel, C. B., W. W. Ballard, S. R. Kimmel, B. Ullmann, and T. F. Schilling. 1995. “Stages of Embryonic Development of the Zebrafish.” *Developmental Dynamics: An Official Publication of the American Association of Anatomists* 203(3):253–310.

Krüger, Monika, Philipp Schledorn, Wieland Schrödl, Hans-Wolfgang Hoppe, Walburga Lutz, and Awad A. Shehata. 2014. “Detection of Glyphosate Residues in Animals and Humans.” *Journal of Environmental & Analytical Toxicology* 4(2):1–5.

Kumar, Vikas, Ajanta Chakraborty, Mool Raj Kural, and Partha Roy. 2009. “Alteration of Testicular Steroidogenesis and Histopathology of Reproductive System in Male Rats Treated with Triclosan.” *Reproductive Toxicology (Elmsford, N.Y.)* 27(2):177–85.

Landrigan, Philip J., and Fiorella Belpoggi. 2018. “The Need for Independent Research on the Health Effects of Glyphosate-Based Herbicides.” *Environmental Health: A Global Access Science Source* 17(1):51.

Li, Qingli, Mark J. Lambrechts, Qiuyang Zhang, Sen Liu, Dongxia Ge, Rutie Yin, Mingrong Xi, and Zongbing You. 2013. “Glyphosate and AMPA Inhibit Cancer Cell Growth

through Inhibiting Intracellular Glycine Synthesis." *Drug Design, Development and Therapy* 7:635–43.

Liu, Binqiu, Yingqiang Wang, Kerry L. Fillgrove, and Vernon E. Anderson. 2002. "Triclosan Inhibits Enoyl-Reductase of Type I Fatty Acid Synthase in Vitro and Is Cytotoxic to MCF-7 and SKBr-3 Breast Cancer Cells." *Cancer Chemotherapy and Pharmacology* 49(3):187–93.

Live, Daily Buzz. 2014. "Chemical Found In Colgate Total Toothpaste Linked To Cancer." *DailyBuzzLive.Com*. Retrieved December 15, 2019 (http://dailybuzzlive.com/chemical-found-colgate-total-toothpaste-linked-cancer/).

Ma, Dong, Ting Wu, Jinglin Zhang, Minsong Lin, Wenjie Mai, Shaozao Tan, Wei Xue, and Xiang Cai. 2013. "Supramolecular Hydrogels Sustained Release Triclosan with Controlled Antibacterial Activity and Limited Cytotoxicity." Retrieved December 15, 2019 (https://www.ingentaconnect.com/content/asp/sam/2013/00000005/00000010/art00010?crawler=true).

Ma, Zhiyuan, Hongling Liu, and Hongxia Yu. 2019. "Triclosan Affects Ca2+ Regulatory Module and Musculature Development in Skeletal Myocyte during Early Life Stages of Zebrafish (Danio Rerio)." *Environmental Science & Technology* 53(20):11988–98.

Martinez, Adriana, and Abraham Jacob Al-Ahmad. 2019. "Effects of Glyphosate and Aminomethylphosphonic Acid on an Isogeneic Model of the Human Blood-Brain Barrier." *Toxicology Letters* 304:39–49.

Meftaul, Islam Md., Kadiyala Venkateswarlu, Rajarathnam Dharmarajan, Prasath Annamalai, Md Asaduzzaman, Aney Parven, and Mallavarapu Megharaj. 2020. "Controversies over Human Health and Ecological Impacts of Glyphosate: Is It to Be Banned in Modern Agriculture?" *Environmental Pollution* 263:114372.

Mesnage, R., B. Bernay, and G. E. Séralini. 2013. "Ethoxylated Adjuvants of Glyphosate-Based Herbicides Are Active Principles of Human Cell Toxicity." *Toxicology* 313(2–3):122–28.

Mesnage, R., N. Defarge, J. Spiroux de Vendômois, and G. E. Séralini. 2015. "Potential Toxic Effects of Glyphosate and Its Commercial Formulations below Regulatory Limits." *Food and Chemical Toxicology: An International Journal Published for the British Industrial Biological Research Association* 84:133–53.

Mesnage, Robin, Alexia Phedonos, Martina Biserni, Matthew Arno, Sucharitha Balu, J. Christopher Corton, Ricardo Ugarte, and Michael N. Antoniou. 2017. "Evaluation of Estrogen Receptor Alpha Activation by Glyphosate-Based Herbicide Constituents." *Food and Chemical Toxicology: An International Journal Published for the British Industrial Biological Research Association* 108(Pt A):30–42.

Miller, T. L., D. J. Lorusso, M. L. Walsh, and M. L. Deinzer. 1983. “The Acute Toxicity of Penta-, Hexa-, and Heptachlorohydroxydiphenyl Ethers in Mice.” *Journal of Toxicology and Environmental Health* 12(2–3):245–53.

Mink, Pamela J., Jack S. Mandel, Bonnielin K. Sceurman, and Jessica I. Lundin. 2012. “Epidemiologic Studies of Glyphosate and Cancer: A Review.” *Regulatory Toxicology and Pharmacology: RTP* 63(3):440–52.

Myers, John Peterson, Michael N. Antoniou, Bruce Blumberg, Lynn Carroll, Theo Colborn, Lorne G. Everett, Michael Hansen, Philip J. Landrigan, Bruce P. Lanphear, Robin Mesnage, Laura N. Vandenberg, Frederick S. Vom Saal, Wade V. Welshons, and Charles M. Benbrook. 2016. “Concerns over Use of Glyphosate-Based Herbicides and Risks Associated with Exposures: A Consensus Statement.” *Environmental Health: A Global Access Science Source* 15:19.

Niemann, Lars, Christian Sieke, Rudolf Pfeil, and Roland Solecki. 2015. “A Critical Review of Glyphosate Findings in Human Urine Samples and Comparison with the Exposure of Operators and Consumers.” *Journal Für Verbraucherschutz Und Lebensmittelsicherheit* 10(1):3–12.

Panzer, Jessica A., Sarah M. Gibbs, Roland Dosch, Daniel Wagner, Mary C. Mullins, Michael Granato, and Rita J. Balice-Gordon. 2005. “Neuromuscular Synaptogenesis in Wild-Type and Mutant Zebrafish.” *Developmental Biology* 285(2):340–57.

Richard, Sophie, Safa Moslemi, Herbert Sipahutar, Nora Benachour, and Gilles-Eric Seralini. 2005. “Differential Effects of Glyphosate and Roundup on Human Placental Cells and Aromatase.” *Environmental Health Perspectives* 113(6):716–20.

Sage, Daniel, Lauréne Donati, Ferréol Soulez, Denis Fortun, Guillaume Schmit, Arne Seitz, Romain Guiet, Cédric Vonesch, and Michael Unser. 2017. “DeconvolutionLab2: An Open-Source Software for Deconvolution Microscopy.” *Methods* 115:28–41.

Saley, Alisha, Megan Hess, Kelsey Miller, David Howard, and Tisha C. King-Heiden. 2016. “Cardiac Toxicity of Triclosan in Developing Zebrafish.” *Zebrafish* 13(5):399–404.

Saunders, Lyndsay E., and Reza Pezeshki. 2015. “Glyphosate in Runoff Waters and in the Root-Zone: A Review.” *Toxics* 3(4):462–80.

Schweizer, H. P. 2001. “Triclosan: A Widely Used Biocide and Its Link to Antibiotics.” *FEMS Microbiology Letters* 202(1):1–7.

Schweizer, Mona, Klaus Brilisauer, Rita Triebskorn, Karl Forchhammer, and Heinz-R. Köhler. 2019. “How Glyphosate and Its Associated Acidity Affect Early Development in Zebrafish (Danio Rerio).” *PeerJ* 7.

Slayden, R. A., R. E. Lee, and C. E. Barry. 2000. “Isoniazid Affects Multiple Components of the Type II Fatty Acid Synthase System of Mycobacterium Tuberculosis.” *Molecular Microbiology* 38(3):514–25.

Sritana, Narongrit, Tawit Suriyo, Jantamas Kanitwithayanun, Benjaporn Homkajorn Songvasin, Apinya Thiantanawat, and Jutamaad Satayavivad. 2018. “Glyphosate Induces Growth of Estrogen Receptor Alpha Positive Cholangiocarcinoma Cells via Non-Genomic Estrogen Receptor/ERK1/2 Signaling Pathway.” *Food and Chemical Toxicology: An International Journal Published for the British Industrial Biological Research Association* 118:595–607.

Stoker, Tammy E., Emily K. Gibson, and Leah M. Zorrilla. 2010. “Triclosan Exposure Modulates Estrogen-Dependent Responses in the Female Wistar Rat.” *Toxicological Sciences: An Official Journal of the Society of Toxicology* 117(1):45–53.

Sulukan, Ekrem, Mine Köktürk, Hamid Ceylan, Şükrü Beydemir, Mesut Işik, Muhammed Atamanalp, and Saltuk Buğrahan Ceyhun. 2017. “An Approach to Clarify the Effect Mechanism of Glyphosate on Body Malformations during Embryonic Development of Zebrafish (Daino Rerio).” *Chemosphere* 180:77–85.

Swanson, Nancy Lee, André Leu, Jon Abrahamson, and B. C. Wallet. 2014. “Genetically Engineered Crops, Glyphosate and the Deterioration of Health in the United States of America.”

Thongprakaisang, Siriporn, Apinya Thiantanawat, Nuchanart Rangkadilok, Tawit Suriyo, and Jutamaad Satayavivad. 2013. “Glyphosate Induces Human Breast Cancer Cells Growth via Estrogen Receptors.” *Food and Chemical Toxicology: An International Journal Published for the British Industrial Biological Research Association* 59:129–36.

Wallace, W., L. H. Schaefer, and J. R. Swedlow. 2001. “A Workingperson’s Guide to Deconvolution in Light Microscopy.” *BioTechniques* 31(5):1076–78, 1080, 1082 passim.

Weatherly, Lisa M., and Julie A. Gosse. 2017. “Triclosan Exposure, Transformation, and Human Health Effects.” *Journal of Toxicology and Environmental Health. Part B, Critical Reviews* 20(8):447–69.

Weatherly, Lisa M., Andrew J. Nelson, Juyoung Shim, Abigail M. Riitano, Erik D. Gerson, Andrew J. Hart, Jaime de Juan-Sanz, Timothy A. Ryan, Roger Sher, Samuel T. Hess, and Julie A. Gosse. 2018. “Antimicrobial Agent Triclosan Disrupts Mitochondrial Structure, Revealed by Super-Resolution Microscopy, and Inhibits Mast Cell Signaling via Calcium Modulation.” *Toxicology and Applied Pharmacology* 349:39–54.

Weatherly, Lisa M., Juyoung Shim, Hina N. Hashmi, Rachel H. Kennedy, Samuel T. Hess, and Julie A. Gosse. 2016. “Antimicrobial Agent Triclosan Is a Proton Ionophore Uncoupler of Mitochondria in Living Rat and Human Mast Cells and in Primary Human Keratinocytes.” *Journal of Applied Toxicology: JAT* 36(6):777–89.

Wolff, Mary S., Susan L. Teitelbaum, Gayle Windham, Susan M. Pinney, Julie A. Britton, Carol Chelimo, James Godbold, Frank Biro, Lawrence H. Kushi, Christine M. Pfeiffer, and Antonia M. Calafat. 2007. “Pilot Study of Urinary Biomarkers of

Phytoestrogens, Phthalates, and Phenols in Girls." *Environmental Health Perspectives* 115(1):116–21.

Wu, Jian-lin, Jie Liu, and Zongwei Cai. 2010. "Determination of Triclosan Metabolites by Using In-Source Fragmentation from High-Performance Liquid Chromatography/Negative Atmospheric Pressure Chemical Ionization Ion Trap Mass Spectrometry." *Rapid Communications in Mass Spectrometry* 24(13):1828–34.

Zhang, Jing-Wen, Ding-Qi Xu, and Xi-Zeng Feng. 2019. "The Toxic Effects and Possible Mechanisms of Glyphosate on Mouse Oocytes." *Chemosphere* 237:124435.

Zhang, Shuhui, Jia Xu, Xiangyu Kuang, Shibao Li, Xiang Li, Dongyan Chen, Xin Zhao, and Xizeng Feng. 2017. "Biological Impacts of Glyphosate on Morphology, Embryo Biomechanics and Larval Behavior in Zebrafish (Danio Rerio)." *Chemosphere* 181:270–80.